ADVANCED OPTICAL MATERIALS
www.advopticalmat.de

Hyperphosphorescent OLEDs: Harnessing the Power of MR-TADF Terminal Emitters

Emma V. Puttock, Janine Haug, Eli Zysman-Colman, and Stefan Bräse*

Hyperphosphorescent organic light-emitting diodes (HP-OLEDs) represent an attractive solution to persistent efficiency roll-off and device stability issues, combining phosphorescent sensitizers with fluorescent terminal emitters to achieve efficient, narrowband emission. This review discusses advances in HP-OLEDs where the terminal emitter is a multiresonance thermally activated delayed fluorescence compound. Recent breakthroughs in device performance, including examples demonstrating both high maximum external quantum efficiencies (EQE_{max}) and excellent color purity, are highlighted. This review summarizes design strategies, challenges, and future directions for improving the efficiency, stability, and spectral performance of HP-OLEDs.

1. Introduction

Organic light-emitting diodes (OLEDs) have emerged as a groundbreaking display and lighting technology, becoming widely used over the past decade in consumer electronics such as mobile phones, smartwatches, and televisions.[1,2] Despite their commercialization, technological hurdles remain, including prolonging operational device lifetimes, and improving color purity for next-generation ultrahigh-definition displays.[3–7]

Achieving a balance between high efficiency, exceptional color purity, and suitably long operational stability remains an outstanding issue, particularly for the blue subpixel,[8] as improvements in one area often come at the expense of another. For example, strategies to enhance device efficiency, such as through the use of materials capable of harvesting 100% of the electrically generated excitons like thermally activated delayed fluorescence (TADF)[9–12] and phosphorescent emitters,[13–17] also frequently lead to concomitant spectral broadening that diminishes color saturation.[18,19] Similarly, efforts to improve the stability of OLEDs often involve compromises in device efficiency.[20–23] These limitations underscore the need for innovative materials and device architectures capable of overcoming the inherent performance trade-offs in OLED technology.

1.1. Hyperphosphorescent OLEDs

Hyperphosphorescent (HP-) OLEDs combine fluorescent emitters (referred to as terminal emitters, TEs) with phosphorescent sensitizers. This device architecture is an enticing potential solution to address the aforementioned outstanding limitations. For this review, we use the term "hyperOLEDs" to collectively describe both hyperfluorescent (HF-) and hyperphosphorescent OLEDs. While HF-devices rely on TADF sensitizers and HP-OLEDs utilize phosphorescent sensitizers, both approaches exploit sensitizer-mediated energy transfer to the TE to achieve high maximum external quantum efficiencies (EQE_{max}), low efficiency roll-off, and excellent color purity.[24–31] Despite their differences, both systems leverage Förster resonance energy transfer (FRET) to the S_1 state of the TE that leads to light emission.[32]

FRET is a non-radiative, long-range energy transfer mechanism governed by dipole–dipole interactions between donor and acceptor compounds, which enables energy to be transferred from the sensitizer, which is responsible for exciton harvesting, to the TE, which is responsible for emission.[33] Enhancing FRET efficiency relies on several factors: i) controlling the distance between donor and acceptor, ii) controlling the magnitude of the spectral overlap between the donor sensitizer and the absorption of the acceptor TE, iii) controlling the relative orientation of the donor emission and the acceptor absorption dipole moments, and iv) enhancing the photoluminescence quantum yield of the donor. These parameters are encapsulated in the Förster radius (R_0), which is defined as the distance between donor and acceptor at which the energy transfer efficiency equals 50%. Since FRET relies solely on spectral overlap, it allows for relatively larger

E. V. Puttock, J. Haug, S. Bräse
Institute of Organic Chemistry
Karlsruhe Institute of Technology (KIT)
Kaiserstrasse 12, 76131 Karlsruhe, Germany
E-mail: emma.puttock@kit.edu

E. V. Puttock, J. Haug, S. Bräse
Institute of Biological and Chemical Systems – Functional Molecular Systems
Karlsruhe Institute of Technology (KIT)
Kaiserstrasse 12, 76131 Karlsruhe, Germany

J. Haug, E. Zysman-Colman
Organic Semiconductor Centre
EaStCHEM School of Chemistry
University of St Andrews
St Andrews, Fife KY16 9ST, UK

The ORCID identification number(s) for the author(s) of this article can be found under https://doi.org/10.1002/adom.202500514

DOI: 10.1002/adom.202500514

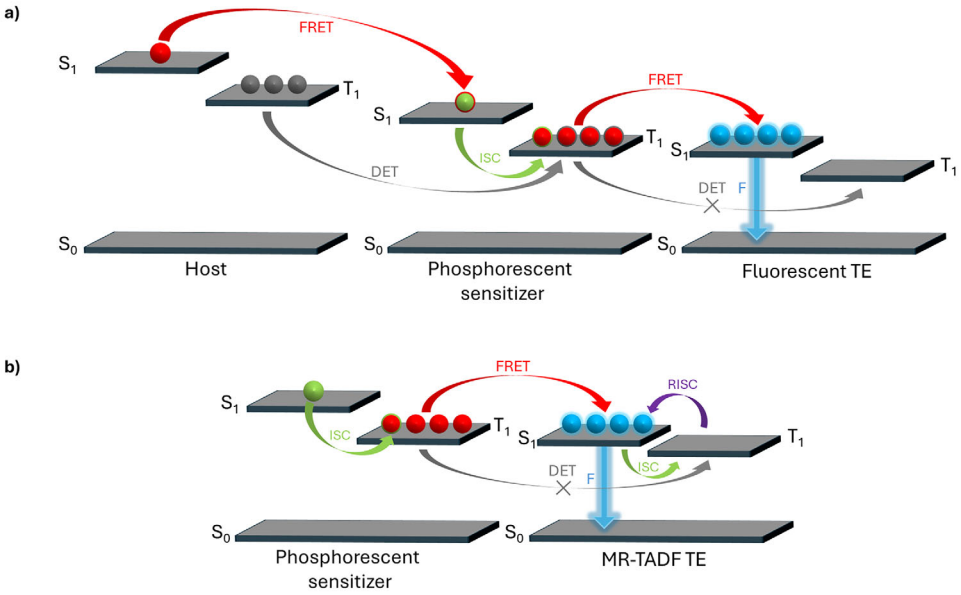

Figure 1. a) Schematic energy diagram of the relaxation pathways in HP devices employing a fluorescent TE (F: fluorescence; ISC: intersystem crossing; FRET: Förster resonance energy transfer, DET: Dexter energy transfer, S_0: singlet ground state, S_1: first excited singlet state, T_1: first excited triplet state). b) Schematic energy diagram of the relaxation pathways in HP devices employing an MR-TADF TE (ISC: intersystem crossing; RISC: reverse intersystem crossing).

spatial separation between the sensitizer and emitter as only the dipoles of the donor and emitter need to be coupled. Maximizing the spectral overlap and increasing R_0 improves energy transfer efficiency, which frequently translates to enhancing device EQE and reducing efficiency roll-off.[34–36]

Notably, FRET is not the only pathway available for energy transfer. Dexter energy transfer (DET), a competing mechanism, operates over much shorter distances (≈1 nm) and involves direct electron exchange between the sensitizer and the TE mediated by both spectra and orbital overlap.[29,37] DET is undesirable in hyperOLEDs as it tends to populate the triplet state of the TE, which is dark and thus prone to non-radiative losses, leading to reduced device efficiency and instability owing to the long-lived nature of these excitons. To suppress DET and optimize FRET, it is essential to carefully control the distance between the sensitizer and TE, primarily engineered through the selection of appropriate doping concentrations. Haase et al. modeled the distances between TADF sensitizers and fluorescent TEs in hyperfluorescent OLEDs as a function of TE doping concentration. Their model showed that within a doping range of 0.3% to 5% TE, the estimated bulk distances (ranging from 3.00 to 1.18 nm) consistently remained above 1 nm, effectively preventing DET.[37] In HP-OLEDs, incorporating sterically demanding groups on the sensitizer or emitter effectively suppresses DET, leading to improved efficiencies.[38–42]

The primary emission mechanism in HP-OLEDs is phosphor-sensitized fluorescence (PSF), a mechanism originally introduced by Baldo et al. in their seminal Nature paper.[31] PSF bridges phosphorescence and fluorescence by enabling efficient exciton harvesting, where triplet excitons generated on the phosphorescent sensitizer are transferred directly to the singlet state of the TE via FRET. This direct triplet-to-singlet transfer mitigates triplet exciton accumulation and reduces non-radiative losses. Consequently, compared to HF-OLEDs, HP devices exhibit enhanced stability and significantly reduced efficiency roll-off at higher luminance (**Figure 1a**),[31,43] making them particularly well-suited for applications demanding both high efficiency and long device lifetimes.[24,44–46]

The fundamental design requirements for efficient hyperphosphorescence are not unique; rather, they mirror those for hyperfluorescent devices.[25,47] Key considerations include i) ensuring spatial separation between the sensitizer and emitter to suppress DET, typically achieved through the use of bulky substituents or low TE concentration,[48,49] ii) maximizing the spectral overlap between the sensitizer's photoluminescence (PL) and the terminal emitter's absorption to improve FRET efficiency,[50] and iii) aligning molecular orbital levels across hosts, sensitizers, and TEs to minimize charge trapping on the TE.[51] These strategies collectively ensure efficient energy transfer.

1.2. Multiresonance-TADF (MR-TADF) Compounds as the Terminal Emitter

MR-TADF compounds have recently emerged as a promising class of emitters, originally introduced as high-color purity alternatives to donor–acceptor TADF emitters.[52] Although their RISC rates are relatively slow,[53–55] this limitation can be mitigated by employing MR-TADF compounds as TEs where their high photoluminescence quantum yields, strong low-energy absorption bands, and narrowband emission can be exploited.[56–60] The inclusion of MR-TADF emitters introduces additional complexity to the energy transfer dynamics in HP devices. Figure 1b provides an overview of the relaxation pathways present in these systems, highlighting the interplay between FRET, and exciton

recycling mediated through intersystem crossing (ISC) and reverse ISC (RISC) cycles, and DET.

1.3. Overview

HP-OLEDs driven by the combination of phosphorescent sensitizers and MR-TADF emitters offer a potentially transformative solution to the challenges faced in OLED technology. These devices typically achieve high efficiency, long lifetimes, and high color purity.

This review focuses on key advancements in HP-OLEDs employing MR-TADF terminal emitters from 2019 to 2025, with an emphasis on the most significant developments and emerging trends, rather than providing an exhaustive overview of all reports. The discussion is structured to first examine Pt-containing sensitizers, followed by Ir-containing sensitizers, as these are the two major classes of phosphorescent complexes used in this field. In addition, we highlight the emerging role of purely organic phosphorescent sensitizers as heavy-metal free sensitizers. Particular attention is given to an analysis of the emissive layer, including sensitizer–emitter combinations and their impact on energy transfer dynamics. By drawing links between energy transfer efficiency and molecular design, we hope to provide insights into how this class of device can be further optimized, potentially pushing the boundaries of OLED technology.

2. Platinum Sensitizers

Though explored in relatively few studies, the integration of Pt-based sensitizers with MR-TADF TEs demonstrates significant potential for enhancing the performance of HP-OLEDs. These systems leverage the distinct properties of platinum complexes, including their strong spin–orbit coupling, ensuring rapid and efficient population of the triplet excited state and enabling FRET to the TE. The use of rigid tetradentate cyclometalated ligand designs,[61] enhances the photostability of these Pt complexes and may contribute to reduced efficiency roll-off by suppressing certain biexcitonic non-radiative decay pathways. Additionally, the square-planar geometry of Pt complexes may enable closer intermolecular packing, potentially enhancing FRET efficiency by reducing donor–acceptor distances. While increased packing could also promote DET and lead to triplet exciton quenching, this can be mitigated through careful molecular design. Ultimately, these characteristics position Pt-based sensitizers as promising choices for high-performance HP-OLEDs.

Son et al. explored the use of **PtON-TBBI**, a well-established solution-processable Pt-complex, as a phosphorescent sensitizer paired with the MR-TADF emitters ***t*-Bu-*ν*-DABNA** and **mBP-DABNA-Me**.[51] The molecular structures of **PtON-TBBI** and the MR-TADF emitters are shown in **Figure 2**. To facilitate an efficient energy transfer process, the TEs were carefully selected to ensure that the triplet energy level of the sensitizer exceeds the singlet energy level of the MR-TADF emitter. This energy alignment is critical for efficient FRET, a cornerstone of the PSF mechanism. The Pt sensitizer was used at a moderately high concentration of 10 wt%, balancing efficient energy transfer with mitigating aggregation, a known weakness of square planar platinum complexes. Furthermore, the concentration of the TE was carefully optimized. Higher concentrations increase the number of emitters within the FRET radius of the sensitizer, thereby enhancing the overall efficiency of energy transfer. However, excessively high concentrations bring the sensitizer and emitters closer, facilitating DET—a competing mechanism discussed in the Introduction—that diminishes device efficiency by accessing non-radiative decay pathways. This optimization was reflected in the photoluminescence quantum yields (PLQYs) of the materials, with the highest values achieved at a doping concentration of 1.0 wt% MR-TADF TE. For instance, PSF films of ***t*-Bu-*ν*-DABNA** achieved a PLQY of 91.1% before dropping to 79.5% at 3.0 wt% doping. Similarly, 1 wt% doping of **mBP-DABNA-Me** has a PLQY of 82.3% compared to 65.6% at 3.0 wt% doping. These trends highlight the importance of optimizing TE concentration to maximize energy transfer while avoiding emission quenching mechanisms at higher concentrations.

The device performance, summarized in **Table 1**, revealed that despite the high PLQYs observed in the films, the overall OLED efficiencies remain modest. Among the pairings, ***t*-Bu-*ν*-DABNA** emerged as the stronger candidate, where the HP-OLED achieved an EQE_{max} of 9.68%, compared to 8.71% for the device using **mBP-DABNA-Me**. This difference was attributed to the larger spectral overlap integral using ***t*-Bu-*ν*-DABNA**, as shown in **Figure 3**, which leads to more efficient energy transfer and resulted in a narrower full width at half maximum (FWHM), 16 nm in PL, 18 nm in electroluminescence (EL). Additionally, the delayed emission lifetimes in the PSF films were significantly shorter when using ***t*-Bu-*ν*-DABNA** (2.1 µs) than with **mBP-DABNA-Me** (8.3 µs), contributing to a less severe efficiency roll-off at higher current densities.

These findings underscore the importance of careful spectral alignment, doping optimization, and exciton management in achieving high-performing HP-OLEDs. The relatively low EQEs—when compared to the maximum theoretical value taking into account their PLQYs—emphasize that while Pt-based sensitizers when paired with MR-TADF TEs having well-matched energy levels show promise, further device optimization is essential to fully capitalize on the potential of these systems.

In a complementary study from Kim et al., **PtON-TBBI** was employed as a sensitizer paired with boron-based MR-TADF TEs containing peripheral electron-donating carbazoles.[62] Two emitters, **TBE01** and **TBE02**, were developed and their performance was compared to that of the reference MR-TADF emitter, ***t*-DABNA** (Figure 2). The modifications to the structures of the TEs were designed to facilitate FRET, while also suppressing DET from nearby molecules such as the exciplex host and sensitizer and mitigating triplet-polaron interactions, both of which contribute to device degradation.

Improved FRET efficiency was demonstrated, with the Förster radius increasing from 3.7 nm for ***t*-DABNA** to 4.2 and 4.5 nm for **TBE01** and **TBE02**, respectively. Codoping with **PtON-TBBI** resulted in shorter emission lifetimes for **TBE01** and **TBE02** (9.3 and 7.2 µs, respectively) relative to ***t*-DABNA** (11.2 µs), indicating a reduction in triplet exciton build-up. These structural modifications also suppressed quenching mechanisms such as triplet–triplet annihilation (TTA), by promoting FRET over DET, thereby minimizing exciton accumulation on the MR-TADF TE. These two emitters also exhibited advantageous photophysical

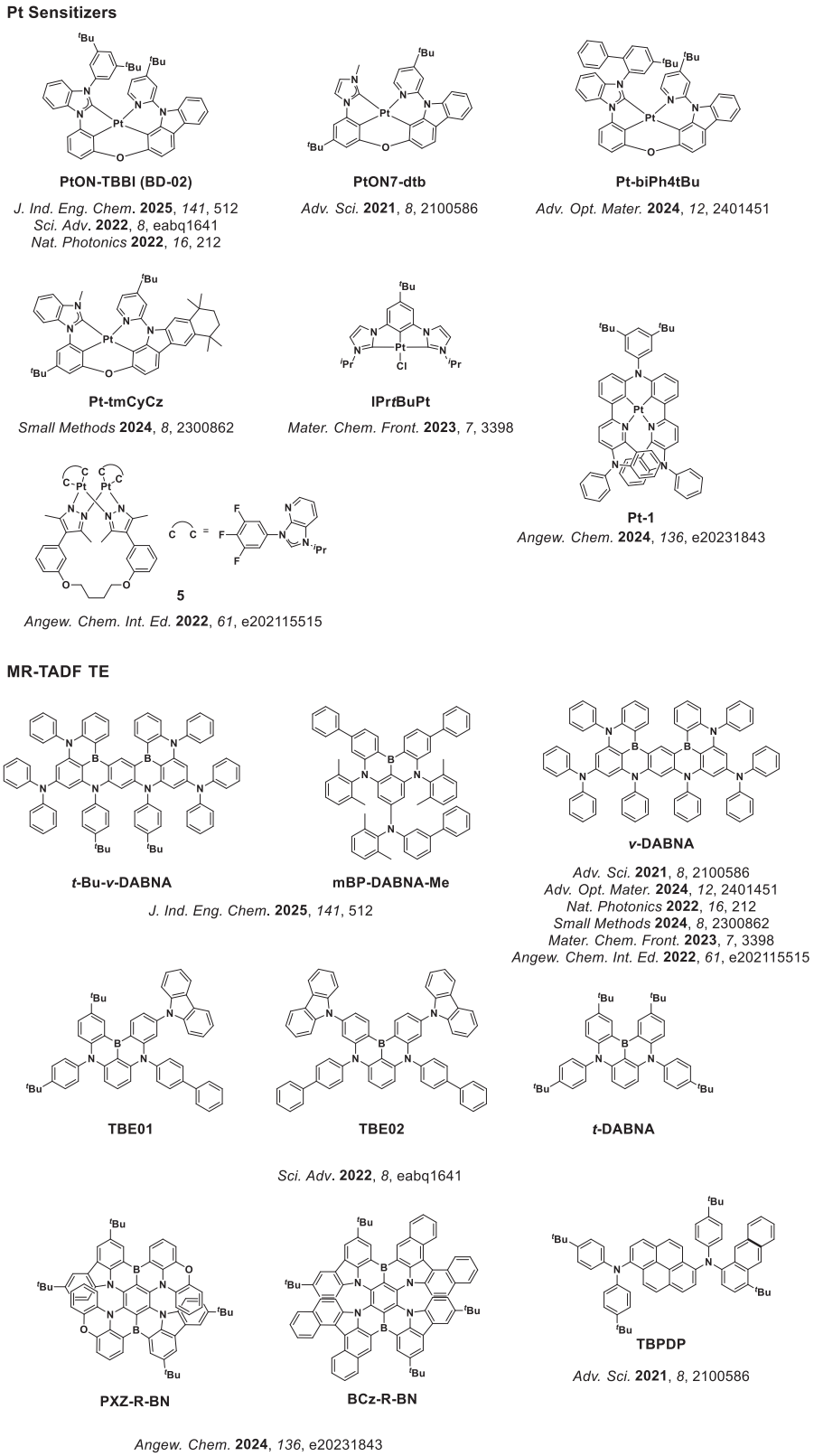

Figure 2. Chemical structures of the Pt-based sensitizers and MR-TADF TEs employed in HP-OLEDs.

Table 1. Key device performance characteristics of HP-OLEDs with platinum-based sensitizers and MR-TADF emitters.

Sensitizer (S)	Terminal emitter (TE)	Composition of emissive layer	Turn-on [V]	EQE_{max} [%]	EQE_{100} [a] [%]	EQE_{1000} [b] [%]	$CIE_{x,y}$	λ_{max} [nm]	Refs.
PtON-TBBI	*t*-Bu-*ν*-DABNA	mCBP-CN:S (10 wt%):TE (0.5 wt%)	5	9.05	–	–	0.12, 0.13	467	[51]
PtON-TBBI	*t*-Bu-*ν*-DABNA	mCBP-CN:S (10 wt%):TE (1 wt%)	5	9.68	–	–	0.12, 0.12	–	
PtON-TBBI	*t*-Bu-*ν*-DABNA	mCBP-CN:S (10 wt%):TE (3 wt%)	5	7.97	–	–	0.12, 0.12	–	
PtON-TBBI	mBP-DABNA-Me	mCBP-CN:S (10 wt%):TE (0.5 wt%)	5.5	8.49	–	–	0.13, 0.13	471	
PtON-TBBI	mBP-DABNA-Me	mCBP-CN:S (10 wt%):TE (1 wt%)	5.5	8.71	–	–	0.13, 0.13	–	
PtON-TBBI	mBP-DABNA-Me	mCBP-CN:S (10 wt%):TE (3 wt%)	5.5	6.42	–	–	0.13, 0.14	–	
PtON-TBBI	*t*-DABNA	SiCzCz:SiTrzCz2 (65:35%):S (13 wt%):TE (0.4 wt%)	–	–	–	23.7	*y* (0.171)		[62]
PtON-TBBI	TBE01	SiCzCz:SiTrzCz2 (65:35%):S (13 wt%):TE (0.4 wt%)	–	–	–	25.4	*y* (0.165)		
PtON-TBBI	TBE02	SiCzCz:SiTrzCz2 (65:35%):S (13 wt%):TE (0.4 wt%)	–	–	–	25.8	*y* (0.165)		
PtON7-dtb	TBPDP[c]	oCBP:mCBP-2CN (1:1):S (10 wt%):TE (0.5 wt%)	–	17.9	–	14.9	0.14, 0.22	474	[34]
PtON7-dtb	TBPDP[c]	oCBP:mCBP-2CN (1:1):S (10 wt%):TE (1.5 wt%)	–	16.9	–	14.3	0.13, 0.27	478	
PtON7-dtb	TBPDP[c]	oCBP:mCBP-2CN (1:1):S (10 wt%):TE (3 wt%)	–	15.0	–	12.2	0.13, 0.31	480	
PtON7-dtb	*ν*-DABNA	oCBP:mCBP-2CN (1:1):S (10 wt%):TE (0.5 wt%)	–	24.9	–	16.5	0.13, 0.14	471	
PtON7-dtb	*ν*-DABNA	oCBP:mCBP-2CN (1:1):S (10 wt%):TE (1.5 wt%)	–	32.2	–	25.4	0.11, 0.14	473	
PtON7-dtb	*ν*-DABNA	oCBP:mCBP-2CN (1:1):S (10 wt%):TE (3 wt%)	–	30.7	–	23.2	0.11, 0.15	475	
Pt-biPh4tBu	*ν*-DABNA	SiCzCz:SiTrzCz2 (59:30%):S (10 wt%):TE (1 wt%)	–	28.6	–	25.6	0.12, 0.12	470	[63]
Pt-tmCyCz	*ν*-DABNA	mCBP:CNmCBP-CN (1:1):S (10 wt%):TE (0.5 wt%)	–	30.5	–	27.5	0.12, 0.12	470	[65]
Pt-tmCyCz	*ν*-DABNA	mCBP:CNmCBP-CN (1:1):S (10 wt%):TE (1 wt%)	–	33.9	–	31.2	0.12, 0.12	472	
IPrtBuPt	*ν*-DABNA	mCBP:SiCzTrz (1:1):S (16 wt%):TE (1 wt%)	–	33.6	–	26.6	0.12, 0.15	471	[49]
Pt-1	PXZ-R-BN	DMIC-TRZ:S (20 wt%):TE (1 wt%)	3.2	29.3	–	–	–	693	[59]
Pt-1	BCz-R-BN	DMIC-TRZ:S (20 wt%):TE (1 wt%)	3.4	24.2	–	–	–	713	
S	*ν*-DABNA	mCBP:S (10 wt%):TE (1 wt%)	–	23.4	–	22.4	0.13, 0.12	469	[70]

[a] External quantum efficiency at 100 cd m^{-2}; [b] External quantum efficiency at 1000 cd m^{-2}; [c] Fluorescent terminal emitter, included for comparison.

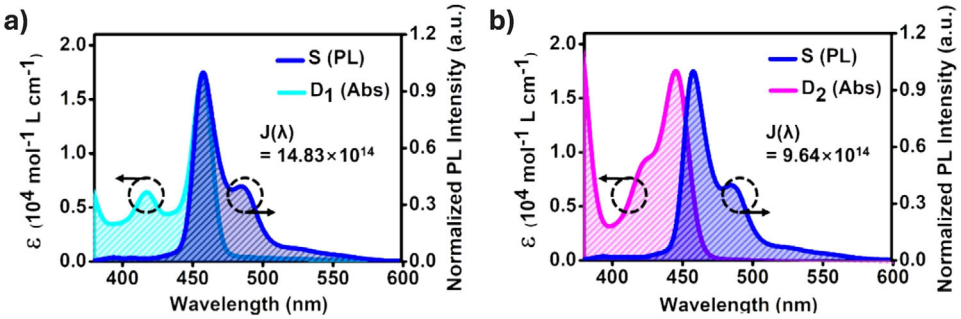

Figure 3. Normalized photoluminescence (PL) spectra and absorption spectra showing overlap integrals for a) ***t*-Bu-*ν*-DABNA** (D_1) and b) **mBP-DABNA-Me** (D_2). Adapted with permission.[51] Copyright 2025, Elsevier.

and charge-transport properties, including higher molar extinction coefficients, faster RISC, and weaker hole-trapping behavior than ***t*-DABNA**.

Despite these desirable properties, FRET was nonetheless relatively inefficient in the PSF devices. This is evidenced by the EL spectra, which exhibited a wider spectral envelope than the TBE emitters alone. These broader spectra arise from the fact that the sensitizer itself contributes a portion of the emission. This can affect both the color purity and the device efficiency. The optimized device configuration utilized 13 wt% **PtON-TBBI** and 0.4 wt% TE. Although not further discussed in this review, as noted by Son et al.[51] the relative and absolute amounts of each codopant play critical roles in maximizing the contribution of the emission from the TE.

Nevertheless, in bottom-emitting configurations, devices using ***t*-DABNA** as the TE achieved an LT_{95} (luminance time—defined as the time required for the device's luminance at 1000 cd m^{-2} to decrease to 95% of its initial value) of 19.8 h with EQE_{1000} of 23.7% and a Commission Internationale de l'Éclairage y-coordinate (CIE)-*y* of 0.171. Devices with **TBE01** as the TE showed a longer lifetime of 42.3 h and a comparable EQE_{1000} of 25.4% and CIE-*y* of 0.165, while devices using **TBE02** showed greater stability, with a device lifetime of 72.9 h, an EQE_{1000} of 25.8% and CIE-*y* of 0.165 (Table 1). This study underscores how molecular design strategies prioritizing FRET over DET, while addressing triplet-polaron interactions and ensuring high energy transfer efficiency can significantly enhance the operational stability and efficiency of HP-OLEDs.

Extending the exploration of Pt-based sensitizers, Nam et al. investigated the closely related **PtON7-dtb** as a sensitizer. They compared its pairing with the MR-TADF emitter ***ν*-DABNA** and the conventional fluorescent emitter **TBPDP** to achieve deep-blue HP-OLEDs.[34] The molecular structures of these compounds are shown in Figure 2. This study highlights the trade-offs involved in using different classes of TEs to optimize OLED performance. The device configuration utilized 10 wt% **PtON7-dtb** and varying concentrations (0.5–3 wt%) of the TE, enabling efficient energy transfer under operational conditions. Controlling charge transport and recombination dynamics were a key focus of the study, with the sensitizer designed to have a higher HOMO level than the TEs. *J*–*V* analysis for hole- and electron-only devices revealed that the sensitizer largely captured injected holes. This localization encouraged trap-assisted recombination, facilitating efficient exciton formation on the sensitizer site. This targeted recombination enables efficient energy transfer to the emitter, reducing charge recombination losses and enhancing overall device efficiency.

Devices using ***ν*-DABNA** demonstrated clear advantages in performance at high luminance levels, achieving an EQE_{1000} of 25.4% with a narrow FWHM of 20 nm, compared to the devices using **TBPDP**, which showed a lower EQE_{1000} of 14.3% and a broader EL, with an FWHM of 51 nm. The device results are summarized in Table 1. The superior EQE and color purity observed for the device using ***ν*-DABNA** highlight the advantages of using MR-TADF TEs. The efficiency roll-off at 1000 cd m^{-2} was improved in the HP-OLEDs for both ***ν*-DABNA** (21.2%) and **TBPDP** (15.1%) compared to the ***ν*-DABNA**-only (29.2%) and **TBPDP**-only (33.5%) OLEDs. Interestingly, the comparison with **TBPDP** highlighted a trade-off between EQE and operational stability. While the MR-TADF TE-containing device achieved higher EQEs, its LT_{50} was 156.3 h. In contrast, the **TBPDP** device achieved a longer LT_{50} of 339.2 h under comparable conditions.

In a related approach, Choi et al. explored the Pt complex, **Pt-biPh4tBu** (Figure 2), which incorporates extended aryl substitution while maintaining the core structural motif of **PtON-TBBI** and **PtON7-dtb**.[63] **Pt-biPh4tBu** was paired with ***ν*-DABNA** at doping concentrations of 10 and 1 wt%, respectively, with the authors citing its substantial spectral overlap and high triplet energy as key factors enabling effective FRET. To examine the effect of the bulky blocking groups in reducing the contribution from DET, HP-OLEDs were additionally fabricated using the structurally related Pt complex **BD-02** (Figure 2),[64] which exhibits PL characteristics similar to **Pt-biPh4tBu**. Both devices showed emission solely from ***ν*-DABNA** in the EL, with a small FWHM of 18 nm. However, the HP-OLED with **Pt-biPh4tBu** demonstrated a slightly enhanced EQE_{1000} of 25.6% (compared to 23.9%), attributed to a reduction in DET. Furthermore, the HP-OLED demonstrated a reduced efficiency roll-off of 10%, 4 percentage points lower than that of the HP-OLED with **BD-02**.

Cheong et al. investigated how the steric effects about the *N*-heterocyclic carbene (NHC)-based tetradentate core of **Pt-tmCyCz** (Figure 2) affects the device performance. This complex contains a cycloalkyl-fused carbazole designed to enhance both rigidity and steric bulk.[65] The complex exhibited resistance to emission quenching, with EL spectra remaining mainly largely unchanged across doping concentrations of 5–20 wt%, with an optimal EQE_{max} of 21.5% observed at 10 wt%. PSF

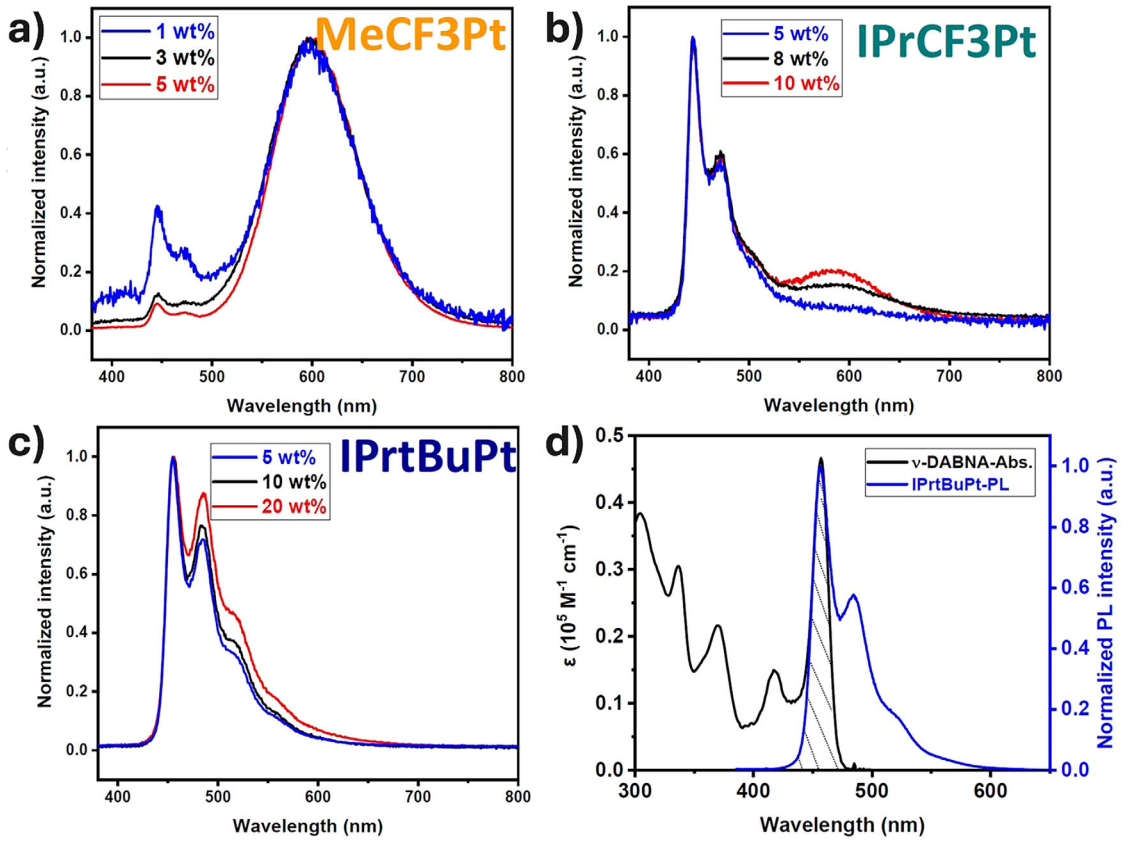

Figure 4. EL spectrum of a) **MeCF3Pt**, b) **IPrCF3Pt**, and c) **IPr*t*BuPt** OLEDs, showing extent of excimer formation with differing concentration. d) Overlap area between UV–vis absorption spectrum of ***ν*-DABNA** and PL spectrum of **IPr*t*BuPt**. Adapted with permission.[49] Copyright 2023, Royal Society of Chemistry.

devices with **Pt-tmCyCz** (10 wt%) and ***ν*-DABNA** (0.5 and 1.0 wt%) demonstrated improved performance compared to the **Pt-tmCyCz**-only devices, with the highest performance achieved at 1.0 wt% ***ν*-DABNA**, resulting in an EQE_{max} of 33.9% and an efficiency roll-off of 8.0% at 1000 cd m^{-2}. The authors attributed the enhanced device stability to the incorporation of the cycloalkyl unit providing steric bulk in concert with a lowering of the HOMO level, which reduces the energy offset with ***ν*-DABNA** and mitigates hole trapping and triplet exciton formation on the TE.

Contributing to the exploration of blue HP-OLEDs, Zhu et al. focused on platinum(II) dicarbene pincer complexes as sensitizers.[49] The strategy of incorporating bulky peripheral groups onto the dicarbene ligand, akin to dendronization,[66] aimed to suppress excimer formation and shorten emission lifetimes by minimizing intermolecular interactions. This approach sometimes allowed doping concentrations to reach up to 20 wt% (**Figure** 4a–c). Incorporating bulky groups also played a role in minimizing DET, further enhancing device performance. The molecular structure of the platinum(II) dicarbene pincer complex **IrPt*t*BuPt** is shown in Figure 2.

The emission of **IPr*t*BuPt** has significant overlap with the absorption of ***ν*-DABNA**, making it a suitable sensitizer in HP-OLEDs (Figure 4d). The device incorporating **IPr*t*BuPt** (16 wt%) and ***ν*-DABNA** (1 wt%) achieved a remarkable EQE_{max} of 33.6%, with a narrow FWHM of 20 nm and CIE coordinates of (0.124, 0.148). In contrast, the device with the **IPr*t*BuPt** emitter alone delivered an EQE_{max} of only 14.0% at 20 wt% doping. The device results are summarized in Table 1.

Notably, the FRET radius for this system was relatively large at 7.1 nm, demonstrating that the steric bulk introduced by the *tert*-butyl groups did not hinder FRET. This HP system achieved both high EQE_{max} and a significantly improved roll-off compared to the device with only **IPr*t*BuPt**, which the authors highlighted as comparable to some of the best-performing HF-OLEDs reported to date. However, it is important to note that the device lifetime (LT_{50}) of the HP-OLED was relatively short at only 0.3 h. This short device lifetime may arise from a combination of factors, including the vulnerability of the Pt—Cl bond to nucleophilic attack, long excited-state lifetime, exciton-induced degradation, and charge imbalance.[67,68]

Extending beyond the typical blue spectrum, Hua et al. developed the Pt-based sensitizer **Pt-1**, specifically designed to pair with the MR-TADF emitters **PXZ-R-BN** and **BCz-R-BN** for narrowband near-infrared (NIR) HP-OLEDs (Figure 2).[59] This sensitizer–emitter pairing exemplifies a carefully targeted synergy, with **Pt-1** engineered to realize significant spectral overlap and efficient energy transfer to the TEs (**Figure** 5).

The devices employed a configuration of 20 wt% **Pt-1** and 1 wt% TE, achieving remarkable efficiencies in the NIR region.

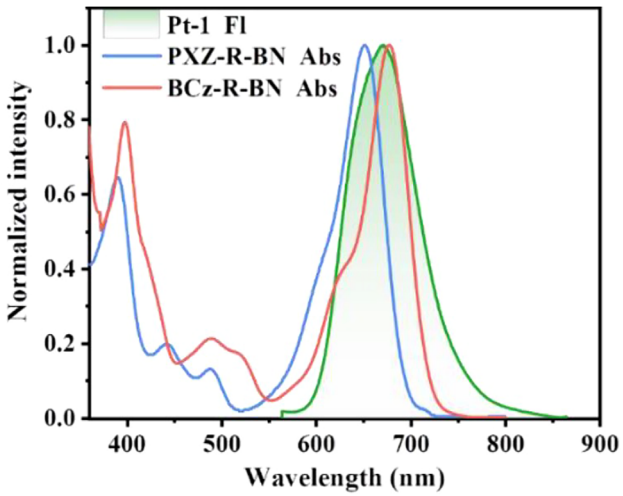

Figure 5. The emission spectrum of sensitizer **Pt-1** and the absorption spectra of **PXZ-R-BN** and **BCz-R-BN** in dilute toluene solution. Reproduced with permission.[59] Copyright 2024, John Wiley and Sons.

The device results are summarized in Table 1. The **PXZ-R-BN** device reached an EQE_{max} of 29.3% at 693 nm, while the device with **BCz-R-BN** achieved an EQE_{max} of 24.2% at 713 nm—a record-breaking efficiency for OLEDs emitting above 700 nm. Notably, devices using **PXZ-R-BN** as the TE demonstrated an LT_{97} of 39 084 h at a radiance of 1000 mW sr^{-1} m^{-2}, based on an acceleration factor of 1.7. While this represents the most stable NIR OLED,[59] direct long-term stability testing at lower luminance remains important for full validation. The study also highlights a significant efficiency roll-off. For example, the **PXZ-R-BN**-based device exhibited efficiencies of 16.8% at 10 mA cm^{-2}, which dropped to 12.0% at 100 mA cm^{-2}, while the **BCz-R-BN**-based device displayed efficiencies of 11.9% at 10 mA cm^{-2}, dropping to 8.0% at 100 mA cm^{-2}. These efficiency roll-offs can be attributed to the build-up of triplet excitons in the device. Triplet excitons may become trapped on the host or sensitizer, also contributing to non-radiative losses and reduced device efficiency under high current densities. Managing the triplet exciton population is a common challenge in OLEDs, where triplet excitons can accumulate on the emitter and contribute to non-radiative decay, leading to loss of performance at high current densities.

Citing the potential for bimetallic complexes to have increased rates of phosphorescent decay,[69] Lo et al. explored a series of dinuclear Pt(II) complexes for high-performance blue phosphorescent OLEDs.[70] Complex **5** (Figure 2), featuring a phenylalkoxy-tethered pyrazole bridge with C^C cyclometallating ligands and bulky iPr groups, exhibited high-thermal stability and efficient blue emission (λ_{PL} = 463 nm and PLQY = 0.94% at 4 wt% in PMMA). Given its favorable spectral overlap with the absorption of ***ν*-DABNA**, photoluminescence decay measurements in mCBP films containing 1 wt% ***ν*-DABNA** and 10 wt% **5** revealed a reduction in the emission lifetime of **5** from 1.3 to 0.5 µs in the co-doped film, suggesting energy transfer to ***ν*-DABNA**. However, the accompanying decrease in the delayed emission lifetime of ***ν*-DABNA** from 4.1 to 1.7 µs in the co-doped film suggested the occurrence of reverse energy transfer from ***ν*-DABNA** back to **5**.

The HP-OLED achieved an EQE_{max} of 23.4%, a narrow FWHM of 18 nm, and a reduced efficiency roll-off of less than 5% at 1000 cd m^{-2} (compared to 10% for the ***ν*-DABNA** control device). The CIE coordinates revealed some contribution from the sensitizer, with the HP-OLED exhibiting a y-coordinate of 0.12 compared to 0.09 for the ***ν*-DABNA**-only device. Nevertheless, the deep-blue HP-OLED demonstrated an LT_{50} of 259 h at 1000 cd m^{-2}, significantly outlasting the ***ν*-DABNA**-only device (LT_{50} = 32.3 h).

These studies collectively highlight that with the right pairing of MR-TADF TEs with Pt-based sensitizers it is possible to achieve remarkable performance in both efficiency and stability in HP-OLEDs while maintaining narrowband emission. Central to these achievements are optimized energy transfer processes, particularly through FRET, and the mitigation of quenching pathways such as Dexter energy transfer and excimer formation. While the progress summarized here is significant, challenges remain, particularly in balancing operational stability with high efficiency at elevated luminance. Continued exploration of spectral alignment, charge recombination dynamics, and emitter stability will be crucial to fully realize the potential of HP OLEDs employing MR-TADF TEs and Pt sensitizers.

3. Iridium Sensitizers

The use of iridium-based sensitizers offers distinct advantages over platinum-based sensitizers that lead to improved performance in MR-TADF TE containing HP-OLEDs. With their relatively shorter excited-state lifetimes and reduced tendency to aggregate compared to platinum-based complexes, iridium complexes are well positioned to efficiently harvest excitons. Recent research efforts have explored the correlation of these attributes to device performance to great effect, yielding strategies that improve device performance across a range of emission wavelengths. The following sections detail developments in iridium-MR-TADF HP-OLEDs, categorized by emission color: blue, green, and red.

3.1. Blue Emission

Lee et al. explored HP-OLEDs as a strategy to tackle the challenges of efficiency roll-off and low luminance in blue OLEDs.[43] This study evaluated three blue phosphorescent sensitizers, **Ir(cb)$_3$**, **F-Ir**, and **CNImIr**, paired with the MR-TADF emitter ***t*-DABNA** (**Figure 6**), aiming to establish the key design requirements for effective sensitization. The authors identified **Ir(cb)$_3$** as the most effective sensitizer, citing its larger spectral overlap integral with ***t*-DABNA** (**Figure 7**a). The energy transfer dynamics were probed by comparing PL spectra for PSF films (Figure 7b). The **Ir(cb)$_3$**-sensitized film has a PL spectrum that closely matches the emission of ***t*-DABNA**, suggesting efficient FRET and negligible back-transfer processes. Interestingly, the **F-Ir**-based film also possesses a comparable emission profile, with a significant alignment to the emission of ***t*-DABNA**. However, the **CNImIr**-sensitized film displays prominent residual phosphor emission, consistent with the authors' conclusions regarding back-transfer mechanisms and suboptimal energy alignment. Transient PL decay measurements were performed to elucidate the energy transfer dynamics. The **Ir(cb)$_3$**-sensitized film

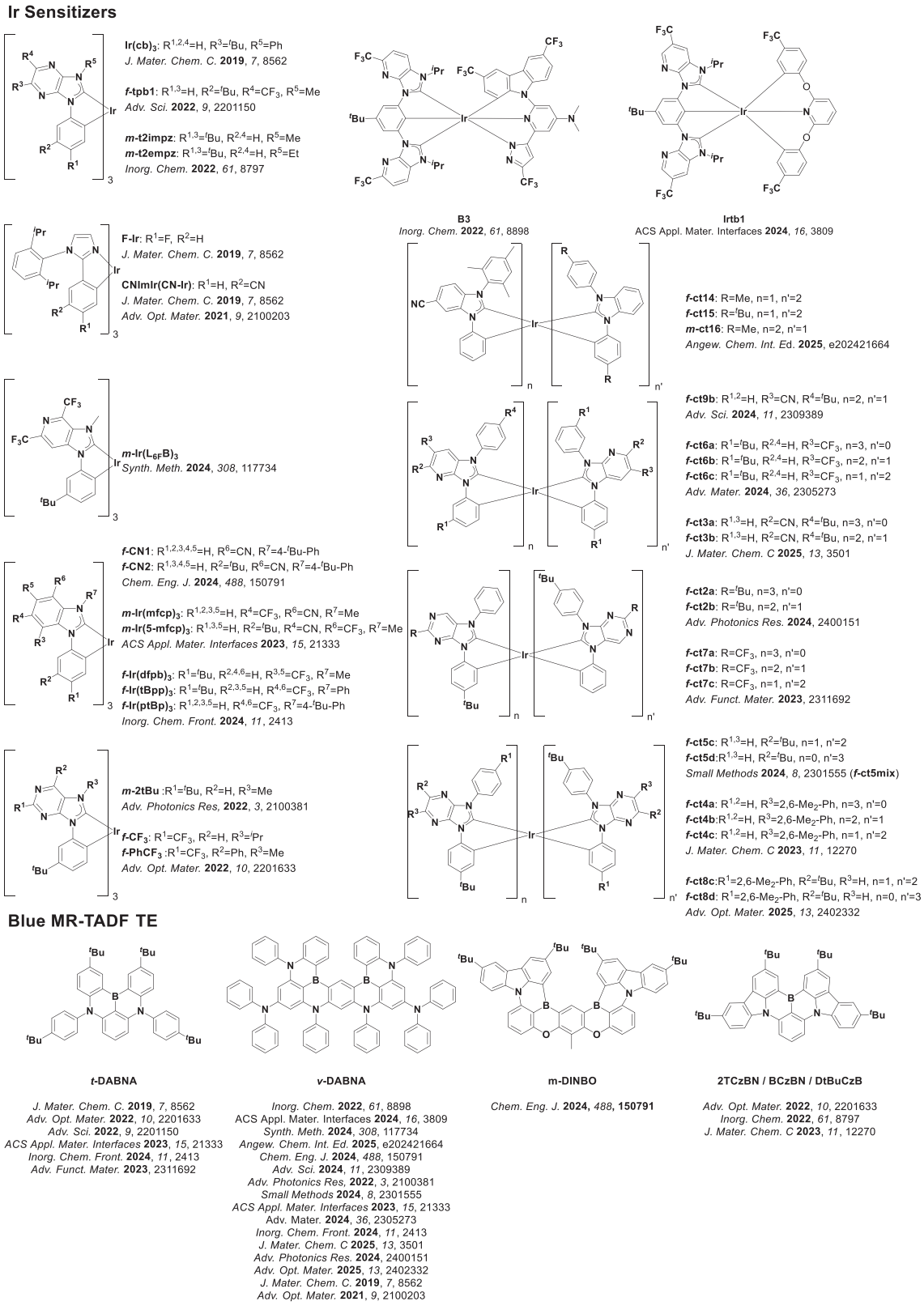

Figure 6. Structures of the Ir-based sensitizers and MR-TADF TEs employed in blue HP-OLEDs.

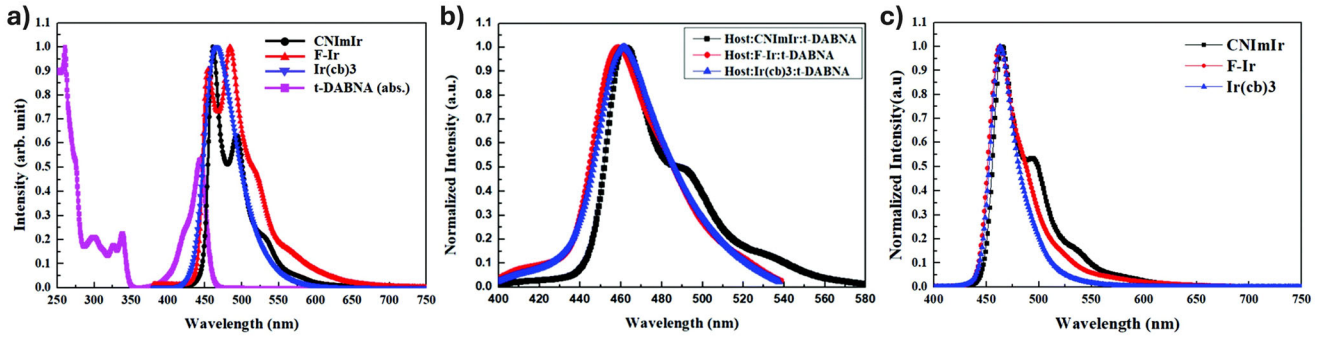

Figure 7. a) Solution PL spectra of the phosphors in toluene compared with the absorption spectrum of ***t*-DABNA**. b) PL spectra of the ***t*-DABNA** doped PSF films. c) EL spectra of HP-OLEDs with different phosphors. Adapted with permission.[43] Copyright 2019, Royal Society of Chemistry.

evidences a fast initial decay characteristic of the prompt fluorescence of ***t*-DABNA**. The **F-Ir**-sensitized films exhibit a slower prompt fluorescence decay compared to **Ir(cb)$_3$**-sensitized films but did show a significantly shorter lifetime relative to the intrinsic PL decay of **F-Ir**, suggesting some FRET does occur.

Despite the promising results from the photophysical study for both **Ir(cb)$_3$**- and **F-Ir**-sensitized films, initial HP-OLEDs fabricated with the sensitizers at concentration of 30 wt% and ***t*-DABNA** at a concentration of 1 wt% revealed surprising mixed emission from the **F-Ir**-sensitized devices (Figure 7c). However, the characteristics of these initial devices were not fully reported. Among the three devices, only the **Ir(cb)$_3$** device showed EL purely from ***t*-DABNA** and therefore was selected as the sensitizer for further study.

The devices comprising 30 wt% **Ir(cb)$_3$** and ***t*-DABNA** demonstrated promising results. While varying ***t*-DABNA** concentrations from 0.5 to 2 wt%, the EQE$_{max}$ remained relatively constant (24.3–24.8%), but the efficiency roll-off was less severe at lower TE doping concentrations. This indicates that the higher doping concentrations likely lead to increased DET and carrier trapping. Notably, the HP-OLEDs exhibited a reduced efficiency roll-off compared to a previously reported hyperfluorescent counterpart, which utilized **DMAC-DPS** as the sensitizer, retaining 79% of the EQE$_{max}$ at 1000 cd m^{-2} versus 65% for the latter.[39] The HP-OLEDs incorporating **Ir(cb)$_3$** exhibited significantly slower degradation, achieving an LT$_{50}$ of 293 h at 200 cd m^{-2}, compared to only 17 h for the ***t*-DABNA** only devices. However, the devices in the stability study used a different host material compared to the devices used in the EQE study, due to the poor stability of the TSPO1 host material in the latter. This exemplifies the difficulty to optimize both device efficiency and stability using a single device stack. Device performance metrics are summarized in **Table 2**.

The Ir(III) complex, **B3**, reported by Zhu et al., offers an example of the less commonly explored bis-tridentate coordination motif (Figure 6).[71] Computational studies indicated that the carbene pincer chelate primarily dominates the electronic transitions associated with the T$_1$ excited state, which has a mixture of LC, MLCT, and ILCT characters. In contrast, the dianionic PzpyCz chelate acts largely as a spectator. **B3** exhibited blue emission (λ_{PL} = 465 nm) with a PLQY of 83% in dichloromethane and a relatively short radiative lifetime of 0.73 µs (τ_{obs} = 0.61 µs). Devices were fabricated using a graded doping profile (16–6 wt% sensitizer), in which the doping concentration decreased linearly from the anode to the cathode. The sensitizer was paired with ***ν*-DABNA** at 1 wt%, chosen for its narrowband emission and high horizontal transition dipole ratio. The resulting HP-OLED achieved an EQE$_{max}$ of 26.2% and CIE$_{xy}$ coordinates of (0.12, 0.14), closely matching other blue HP-OLEDs in this review. Nevertheless, Gaussian fitting of the electroluminescence spectrum revealed a 15% contribution from phosphorescence originating from **B3**, indicating incomplete energy transfer. Increasing the TE concentration to 2 wt% did not eliminate this residual emission, which the authors attributed to a partially allowed FRET pathway and the fast-radiative decay of **B3** enabling direct emission prior to transfer.

A related complex, **Irtb1**, was reported in a subsequent study by Yan et al., featuring a carbene-based pincer ligand with the CF$_3$ group located *meta* to the pyridine chelate, instead of *ortho* as in **B3**, and a 2,6-diaryloxy pyridine ancillary ligand (Figure 6).[72] This altered coordination environment resulted in a blue shifted emission (λ_{max} = 448 nm), a reduced PLQY of 21.8% in toluene and a longer radiative lifetime of 1.93 µs (τ_{obs} = 421 ns). HP-OLEDs fabricated using **Irtb1** as the sensitizer at 28 wt% paired with ***ν*-DABNA** at 1 wt% showed an increased EQE$_{max}$ of 23.5% compared to 20.7% for the unsensitized MR-TADF OLED device. Notably, the efficiency roll-off was much reduced, with an EQE$_{1000}$ of 16.1%, versus 5.1% for the reference device.

Yan et al. paired the green emitting ***m*-Ir(L$_{6F}$B)$_3$** with ***ν*-DABNA** as the terminal emitter.[46] The homoleptic tris-bidentate complex contained NHC carbene chelates coordinated as the *mer* isomer (Figure 6). ***m*-Ir(L$_{6F}$B)$_3$** exhibited broad green emission (λ_{max} = 512 nm), a PLQY of 43%, and a short radiative lifetime of 0.75 µs (τ_{obs} = 0.32 µs) in toluene. Despite the relatively small spectral overlap, ***m*-Ir(L$_{6F}$B)$_3$** acted as a relatively efficient sensitizer of ***ν*-DABNA**, as confirmed by the intense ***ν*-DABNA** emission band observed at 468 nm, accompanied by a low-energy tail from the Ir(III) sensitizer. The HP-OLED, using ***m*-Ir(L$_{6F}$B)$_3$** at 20 wt% and ***ν*-DABNA** at 1 wt%, achieved an EQE$_{max}$ of 25.5%, an improvement over the non-sensitized device (EQE$_{max}$ = 20.3%). Remarkably, the ***m*-Ir(L$_{6F}$B)$_3$**-sensitized device exhibited a much longer LT$_{50}$, approximately three times longer than the equivalent device when sensitized by the blue emitting ***f*-Ir(L$_{6F}$B)$_3$**. However, the CIE-coordinates of the device were (0.17, 0.20), straying from those required for deep blue emission.

Table 2. Key device performance characteristics of hyperphosphorescent OLEDs with iridium-based sensitizers and MR-TADF emitters.

Sensitizer (S)	Terminal emitter (TE)	Composition of emissive layer	Turn-on [V]	EQE_{max} [%]	EQE_{100} [a] [%]	EQE_{1000} [b] [%]	$CIE_{x,y}$	λ_{max} [nm]	Refs.
Blue emission									
$Ir(cb)_3$	*t*-DABNA	TSPO1:S (30 wt%):TE (0.5 wt%)	–	24.6	–	19.4	0.13, 0.12	–	[43]
$Ir(cb)_3$	*t*-DABNA	TSPO1:S (30 wt%):TE (1 wt%)	–	24.8	–	18.4	0.13, 0.11	–	
$Ir(cb)_3$	*t*-DABNA	TSPO1:S (30 wt%):TE (2 wt%)	–	24.3	–	16.3	0.13, 0.11	–	
B3	*ν*-DABNA	PPT:S(16–6 wt%):TE (1 wt%)	4.0	26.2	22.2	17.9	0.12, 0.14	473	[71]
Irtb1	*ν*-DABNA	PPF:S (28 wt%):TE (1 wt%)	3.8	23.5	19.7	16.1	0.12, 0.15	472	[72]
m-$Ir(L_{6F}B)_3$	*ν*-DABNA	SiCzCz:SiTrzCz2:S (20 wt%):TE (1 wt%)	2.8	25.2	–	22.7	0.17, 0.20	468	[46]
f-ct14	*ν*-DABNA	PPF:S (30 wt%):TE (1 wt%)	3.2	32.7	-	27.1	0.12, 0.12	473	[38]
f-ct14	*ν*-DABNA	PPF:S (30 wt%):TE (2 wt%)	3.2	30.9	-	25.5	0.11, 0.14	474	
f-ct15	*ν*-DABNA	PPF:S (30 wt%):TE (1 wt%)	3.3	30.2	-	22.7	0.12, 0.11	471	
f-ct15	*ν*-DABNA	PPF:S (30 wt%):TE (2 wt%)	3.2	32.9	-	26.5	0.12, 0.13	473	
m-ct16	*ν*-DABNA	PPF:S (30 wt%):TE (1 wt%)	3.2	32.9	-	32.1	0.13, 0.16	471	
m-ct16	*ν*-DABNA	PPF:S (30 wt%):TE (2 wt%)	3.2	28.8	-	28.1	0.12, 0.15	472	
f-CN1	*ν*-DABNA	mCPCN:S (30 wt%):TE (1 wt%)	2.8	30.3	27.2	19.6	0.12, 0.16	474	[74,80]
f-CN1	*m*-DINBO	mCPCN:S (30 wt%):TE (1 wt%)	2.8	30.8	26.9	14.7	0.13, 0.10	467	
f-CN2	*ν*-DABNA	mCPCN:S (30 wt%):TE (1 wt%)	2.9	30.6	29.7	20.4	0.13, 0.18	473	
f-CN2	*m*-DINBO	mCPCN:S (30 wt%):TE (1 wt%)	2.8	30.1	27.6	15.9	0.14, 0.13	467	
f-ct9b	*ν*-DABNA	SiCzCz:SiTrzCz2 (65%:35%):S (20 wt%):TE (1 wt%)	2.9	32.1	–	25.5	0.13, 0.12	468	[80]
f-ct9b	*ν*-DABNA	SiCzCz:SiTrzCz2 (65%:35%):S (20 wt%):TE (2 wt%)	2.9	34.7	–	23.0	0.12, 0.13	469	
f-ct9b	*ν*-DABNA	SiCzCz:SiTrzCz2 (65:35%): S (20 wt%):TE (3 wt%)	2.9	30.1	–	15.4	0.12, 0.15	471	
m-2tBu	*ν*-DABNA	PPF:S (14 wt%):TE (2 wt%)	3.5	19.6	19.0	15.6	0.12, 0.16	472	[82]
m-2tBu	*ν*-DABNA	PPF:S (25 wt%):TE (2 wt%)	3.5	22	18.9	14.9	0.12, 0.155	472	
m-2tBu	*ν*-DABNA	PPF:S (40 wt%):TE (2 wt%)	3.5	21.7	17.8	6.9	0.12, 0.16	472	
f-ct5mix	*ν*-DABNA	CzSi:S (10 wt%):TE (1 wt%)	3.6	32	23.3	20.1	0.13, 0.10	–	[87]
f-ct5mix	*ν*-DABNA	CzSi: S (10 wt%): TE (2 wt%)	3.6	27.1	19.5	14.4	0.12, 0.10	–	
f-ct5mix	*ν*-DABNA	CzSi:S (12.5 wt%):TE (1 wt%)	3.5	30.8	23.8	17.9	0.12, 0.10	–	
f-ct5mix	*ν*-DABNA	CzSi: S (12.5 wt%): TE (2 wt%)	3.5	24.5	20.8	15.7	0.13, 0.10	–	
f-ct5mix	*ν*-DABNA	SiCzCz:SiTrzCZ2 (1:1):S (10 wt%):TE (1 wt%)	2.7	30.3	30.1	25.5	0.12, 0.13	–	
f-ct5mix	*ν*-DABNA	SiCzCz:SiTrzCZ2 (1:1): S (12.5 wt%): TE (1 wt%)	2.7	28.1	27.8	24.1	0.12, 0.14	–	
f-CF_3	*t*-DABNA	mCBP:S (15 wt%):TE (3 wt%)	5.2	23.8	16.1	11.4	0.13, 0.14	464	[79]
f-$PhCF_3$	2TCzBN	mCBP:S (15 wt%):TE (3 wt%)	5.4	24	14.3	10.8	0.11, 0.36	485	
f-t2impz	BCzBN	mCP: S (10 wt%): TE (0.5 wt%)	–	13.7	–	–	012, 0.30	485	[85]
f-t2impz	BCzBN	mCP:S (10 wt%):TE (1 wt%)	–	13.8	–	–	0.11, 0.35	485	
f-t2empz	BCzBN	mCP:S (10 wt%):TE (0.5 wt%)	–	17.4	–	–	0.12, 0.30	485	

(*Continued*)

Table 2. (Continued)

Sensitizer (S)	Terminal emitter (TE)	Composition of emissive layer	Turn-on [V]	EQE_{max} [%]	EQE_{100} [a] [%]	EQE_{1000} [b] [%]	$CIE_{x,y}$	λ_{max} [nm]	Refs.
f-t2empz	BCzBN	mCP:S (10 wt%):TE (1 wt%)	–	12.6	–	–	0.11, 0.34	485	
f-tpb1	*t*-DABNA	mCP:S (30 wt%):TE (1 wt%)	4.6	29.6	–	–	0.13, 0.11	462	[76]
f-Ir(mfcp)$_3$	*ν*-DABNA	PPT:S (20 wt%):TE (1 wt%)	4	16.7	–	11.4	0.13, 0.18	473	[78]
f-Ir(mfcp)$_3$	*ν*-DABNA	PPT:S (20 wt%):TE (2 wt%)	4	15.5	–	10.3	0.12, 0.17	474	
f-Ir(mfcp)$_3$	*t*-DABNA	PPT:S (20 wt%):TE (1 wt%)	4	16.1	–	9.7	0.14, 0.18	463	
f-Ir(mfcp)$_3$	*t*-DABNA	PPT:S (20 wt%):TE (2 wt%)	4	15.3	–	8.4	0.14, 0.15	463	
f-Ir(5-mfcp)$_3$	*ν*-DABNA	PPT:S (20 wt%):TE (1 wt%)	4	18.8	–	13.1	0.13, 0.20	473	
f-Ir(5-mfcp)$_3$	*ν*-DABNA	PPT:S (20 wt%):TE (2 wt%)	4	17.1	–	11.4	0.12, 0.18	475	
f-Ir(5-mfcp)$_3$	*t*-DABNA	PPT: S (20 wt%): TE (1 wt%)	4	16.8	–	10.4	0.15, 0.23	465	
f-Ir(5-mfcp)$_3$	*t*-DABNA	PPT:S (20 wt%):TE (2 wt%)	4	16	–	9.1	0.15, 0.18	465	
f-ct4a	DtBuCzB	PPT:S (20 wt%):TE (1 wt%)	5.6	15.3	–	8.5	0.12, 0.41	489	[83]
f-ct4a	DtBuCzB	PPT:S (20 wt%):TE (2 wt%)	5.6	15	–	9.2	0.11, 0.42	489	
f-ct4b	DtBuCzB	PPT:S (20 wt%):TE (1 wt%)	5	21.5	–	14.7	0.11,0.44	490	
f-ct4b	DtBuCzB	PPT:S (20 wt%):TE (2 wt%)	5	20.8	–	14.2	0.11, 0.44	490	
f-ct4c	DtBuCzB	PPT:S (20 wt%):TE (1 wt%)	5.3	17.5	–	11.3	0.11, 0.40	489	
f-ct4c	DtBuCzB	PPT:S (20 wt%):TE (2 wt%)	5.3	17	–	10.6	0.11, 0.44	490	
f-ct6a	*ν*-DABNA	PPF:S (20 wt%):TE (1 wt%)	3.4	26.2	21.6	18.4	0.12, 0.13	472	[75]
f-ct6b	*ν*-DABNA	PPF:S (20 wt%):TE (1 wt%)	3.3	25.1	20.7	17.7	0.12, 0.13	472	
f-ct6c	*ν*-DABNA	PPF: S (20 wt%): TE (1 wt%)	3.3	25.8	21.5	17.3	0.12, 0.13	472	
f-Ir(dfpb)3	*ν*-DABNA	PPT:S (20 wt%):TE (1 wt%)	4.7	14.3	–	7.2	0.12, 0.19	475	[86]
f-Ir(dfpb)3	*t*-DABNA	PPT:S (20 wt%):TE (1 wt%)	4.7	14.3	–	4.5	0.13, 0.12	466	
f-Ir(tBpp)3	*ν*-DABNA	PPT:S (20 wt%):TE (1 wt%)	3.9	18.9	–	11.6	0.12, 0.15	474	
f-Ir(tBpp)3	*t*-DABNA	PPT:S (20 wt%):TE (1 wt%)	3.8	18.1	–	9.7	0.14, 0.10	462	
f-Ir(ptBp)3	*ν*-DABNA	PPT:S (20 wt%):TE (1 wt%)	3.9	16.3	–	9.4	0.12, 0.13	473	
f-Ir(ptBp)3	*t*-DABNA	PPT:S (20 wt%):TE (1 wt%)	3.9	14.1	–	5.2	0.14, 0.10	461	
f-ct3a	*ν*-DABNA	CzSi:S (12.5 wt%):TE (1 wt%)	3.6	25.6	21.9	17.7	0.12, 0.14	468	[73]
f-ct3b	*ν*-DABNA	CzSi:S (12.5 wt%):TE (1 wt%)	3.7	29	23.1	18.5	0.12, 0.13	468	
f-ct2a	*ν*-DABNA	PPF:S (21 vol%):TE (1 vol%)	3.3	22.2	19.4	–	0.12, 0.14	472	[84]
f-ct2b	*ν*-DABNA	PPF:S (21 vol%):TE (1 vol%)	3.2	20.4	13.7	–	0.12, 0.14	472	
f-ct8c	*ν*-DABNA	CzSi:S (10 wt%):TE (1 wt%)	3.6	30.5	21.7	–	0.13, 0.08	468	[77]
f-ct8d	*ν*-DABNA	CzSi:S (10 wt%):TE (1 wt%)	3.8	26.3	20.7	–	0.13, 0.08	468	
f-ct8c	*ν*-DABNA	SiCzCz:SiTrzCZ2 (1:1): S (10 wt%): TE (1 wt%)	2.8	28.4	–	23.6	0.12, 0.15	472	
f-ct8d	*ν*-DABNA	SiCzCz:SiTrzCZ2 (1:1):S (10 wt%):TE (1 wt%)	2.8	28.1	–	24.1	0.12, 0.15	472	
f-ct7a	*t*-DABNA	PPT:S (25 wt%):TE (1.5 wt%)	4.1	32.5	–	14.9	0.14, 0.09	460	[81]
f-ct7b	*t*-DABNA	PPT:S (25 wt%):TE (1.5 wt%)	3.9	36.1	–	13.3	0.14, 0.09	460	
f-ct7c	*t*-DABNA	PPT:S (25 wt%):TE (1.5 wt%)	4.1	26.4	–	12.4	0.14, 0.09	460	

(*Continued*)

Table 2. (Continued)

Sensitizer (S)	Terminal emitter (TE)	Composition of emissive layer	Turn-on [V]	EQE_{max} [%]	EQE_{100} [a] [%]	EQE_{1000} [b] [%]	$CIE_{x,y}$	λ_{max} [nm]	Refs.
CN-Ir	*ν*-DABNA	mCBP:SiCz2TRz (1:1): S (20 wt%): TE (0.5 wt%)	3	27.3	–	23.3	0.13, 0.16	470	[88]
Green emission									
$Ir(ppy)_3$	AZA-BN	mCBP:S (30 wt%):TE (6 wt%)	2.6	28.2	26.5	19.1	0.27, 0.69	527	[56]
$Ir(ppy)_2acac$	BpIC-DPA	DIC-TRZ:S (5 wt%):TE (2 wt%)	2.4	22	–	18.6	0.3, 0.67	536	[89]
$Ir(ppy)_2acac$	BpIC-Cz	DIC-TRZ: S (5 wt%): TE (4 wt%)	2.4	25.7	–	24.3	0.34, 0.64	544	
5tBuCzBN[c]	BN-TPP	PhCzBCz:S (20 wt%):TE (2 wt%)	–	24.3	24.2	21.9	0.11, 0.39	492	[90]
$Ir(ppy)_3$	BN-DPBQ	PhCzBCz:S (8 wt%):TE (2 wt%)	–	22.8	20.8	16.3	0.32, 0.66	538	
$Ir(ppy)_3$	PhCzBN-PO	DMIC-TRZ:S (20 wt%):TE (1 wt%)	2.6	32.4	32.3	31.4	0.24, 0.67	513	[93]
$Ir(ppy)_3$	*m*-DBCz	PhCzBCz:S (20 wt%):TE (1 wt%)	2.8	36.7	–	32.2	0.33, 0.65	544	[60]
$Ir(ppy)_3$	*m*-DBCz	DMIC-TRZ:S (20 wt%):TE (1 wt%)	2.4	36.3	–	35.1	0.35, 0.63	548	
$Ir(ppy)_3$	PXZ-tCzBN	DIC-TRZ:S (20 wt%):TE (5 wt%)	2.2	20.7	20.5	18.8	0.31, 0.64	524	[35]
$Ir(ppy)_3$	PhPXZ-tCzBN	DIC-TRZ:S (20 wt%):TE (5 wt%)	2.15	27.6	27.4	25.7	0.35, 0.63	536	
$Ir(ppy)_3$	MesPXZ-tCzBN	DIC-TRZ:S (20 wt%):TE (5 wt%)	2.1	27.6	27.3	25.5	0.31. 0.65	528	
Red emission									
$Ir(mphmq)_2tmd$	BN-R	NPB:DMFBD-TRZ(2:1):S (3 wt%):TE (1 wt%)	2.9	20.1	16.4	13.3	0.66, 0.34	618	[58]
$Ir(piq)_2acac$	BNNO	DMIC-TRZ:S (8 wt%):TE (1 wt%)	2.7	34.4	–	31.4	0.71, 0.29	643	[94]
$Bt_2Ir(acac)$	B4N6-Me	DMIC-TRZ:S (10 wt%):TE (1 wt%)	2.7	35.8	–	28.4	0.57, 0.43	588	[57]
$Bt_2Ir(acac)$	B4N6-Me	DMIC-TRZ:S (10 wt%):TE (1.5 wt%)	2.7	35.1	–	21.6	0.57, 0.43	588	
$Bt_2Ir(acac)$	B4N6-Me	DMIC-TRZ:S (10 wt%):TE (2 wt%)	2.7	34.3	–	18.3	0.57, 0.43	588	

[a] External quantum efficiency at 100 cd m^{-2}; [b] External quantum efficiency at 1000 cd m^{-2}; [c] TADF sensitizer, included for comparison.

A substantial body of work by Chi and co-workers has established a wide range of NHC iridium(III) complexes as phosphorescent sensitizers for HP-OLEDs.[38,73–87] While the reported complexes differ in peripheral substitution and electronic tuning, they are unified by a conserved tris-bidentate coordination framework, in which each ligand contributes a carbene and a carbon donor. This structural consistency enables comparisons (Table 2 and Figure 6), while also revealing how even subtle changes to the sensitizer framework—such as peripheral substitution or ligand rigidity—fine-tunes the photophysical properties of the complex. These variations, in turn, impact the choice of host selection, doping concentration, and terminal emitter pairing, ultimately influencing device performance. Although this consistency allows us to identify recurring design trends, direct comparison across studies is complicated by differences in host materials, terminal emitters, and doping strategies. We highlight here representative examples that illustrate key design principles.

Among the highest-performing devices are those by Wu et al., which employ heteroleptic Ir(III) complexes featuring two distinct carbene chelates bearing *N*-aryl substituents.[38] These complexes, ***f*-ct14**, ***f*-ct15**, ***m*-ct16**, were used at a sensitizer concentration of 30 wt% in combination with ***v*-DABNA** (1 or 2 wt%). These systems achieved narrowband emission (FWHM 19 nm, 0.11 eV) and EQE_{max} values exceeding 30%, with the device with ***m*-ct16** also displaying excellent roll-off suppression (EQE_{1000} of 32.1% and EQE_{10000} of 27.7%). The authors attributed the high performance to rapid phosphorescent decay, which may reduce triplet accumulation and the probability of DET. However, as no emission from the sensitizer was observed in the EL, the precise contribution of the fast radiative decay from the sensitizer remains open to interpretation.

Yan et al. introduced the homoleptic Ir(III) carbene complexes ***f*-CN1** and ***f*-CN2** as phosphorescent sensitizers paired with the MR-TADF emitters ***v*-DABNA** and ***m*-DINBO**.[74] Incorporating 1 wt% of the TE and 30 wt% of the phosphorescent sensitizer, each Ir(III)-MR-TADF pairing showed high PLQY (100%) and small FWHM values (18–22 nm). Despite similar EQE_{max} values across all devices (30.1–30.8%), performance diverged markedly at higher luminance. Devices employing ***v*-DABNA** exhibited superior efficiency roll-off characteristics, with the ***f*-CN1**/***v*-DABNA** device maintaining an EQE_{1000} of 19.6%, compared to just 14.7% for the ***f*-CN1**/***m*-DINBO** device counterpart. A similar trend was observed in the ***f*-CN2** devices, where the ***v*-DABNA**-based device likewise outperformed the ***m*-DINBO**-based device at elevated brightness levels. This behavior was attributed to enhanced exciton recycling in the ***v*-DABNA**-based systems, where efficient RISC on the TE facilitates the conversion of non-radiative triplet excitons into radiative singlets. Additionally, slightly better spectral overlap and frontier orbital alignment with the Ir(III) complex may contribute to more efficient energy transfer.

Wu et al. reported ***f*-ct9b**, a bulky Ir(III) complex featuring an NHC chelate with two *N*-aryl substituents, which can bind through either of its rings.[80] PSF devices were fabricated with 20 wt% sensitizer and varying concentrations of ***v*-DABNA**. At 1 wt% TE, the device achieved an EQE_{max} of 32.1% and EQE_{1000} of 25.5%. Increasing the TE concentration to 2 wt% led to a maximum EQE of 34.7%, although the EQE_{1000} dropped slightly to 23%. At 3 wt% TE, both metrics declined further (EQE_{max} = 30.1%, EQE_{1000} = 15.4%), suggesting the onset of concentration quenching from increased non-radiative losses.

Across these high-performing systems, a recurring feature is the use of NHC ligands bearing dual *N*-aryl substituents. As noted by Wu et al., this design is thought to enhance molecular rigidity and stability through stronger N—C(aryl) bonds, while also promoting shorter radiative lifetimes that may mitigate exciton annihilation in the device at high current density.[80] These structural features likely contribute to the consistently high EQE_{max} and mild efficiency roll-off observed across the most efficient devices, particularly when paired with well-matched hosts and terminal emitters at suitable doping levels, and may also help suppress undesired DET by spatially isolating the sensitizer molecules in the emissive layer.

Jin et al. explored the blue-emitting iridium complex ***m*-2tBu**, which contains a tris-bidentate framework with one ligand bearing an *N*-alkyl (methyl) substituent and the other an *N*-aryl substituent.[82] In contrast to the dual bulky aryl substitution used in the most efficient systems, this less sterically demanding structure may account for a more modest EQE_{max}. Nevertheless, the study offers a rare perspective on sensitizer doping concentration. Paired with ***v*-DABNA** (2 wt%), the doping concentration of ***m*-2tBu** was varied from 14% to 40 wt%. The FRET from the sensitizer proved to be highly efficient, regardless of sensitizer concentration. The devices exhibited a narrow FWHM of 21 nm, reflecting the spectral purity of the emission solely from the TE. Incorporating bulky *tert*-butyl groups within ***m*-2tBu** proved instrumental in reducing the likelihood of DET. At an optimized concentration of 25 wt% sensitizer and 2 wt% TE, the device achieved an EQE_{max} of 22.0%—an improvement over the 17% obtained from the sensitizer-only device. While the *tert*-butyl groups were proposed to mitigate DET by limiting intermolecular interactions, the devices still exhibited significant efficiency roll-off (≈32%) from peak performance to 1000 cd m^{-2}.

A final notable example comes from Yan et al., who reported the iridium complex ***f*-ct5mix**, a chromatographically inseparable mixture of ***f*-ct5c** and ***f*-ct5d** in a 3:4 ratio.[87] Devices incorporating ***f*-ct5mix** as the sensitizer and ***v*-DABNA** as the TE were fabricated using various host materials and doping concentrations. In a CzSi host at 10 wt% sensitizer and 1 wt% TE, the device achieved an EQE_{max} of 32.0%. Increasing the sensitizer concentration to 12.5 wt% resulted in only a modest reduction in EQE_{max} (30.8%) indicating that performance was relatively insensitive to this parameter. However, raising the terminal emitter concentration from 1 to 2 wt% had a more pronounced impact, with EQE_{max} dropping to 27.1% (and to 24.5% at 12.5 wt% sensitizer), likely due to an increase in DET. In a SiCzCz:SiTrzCZ2 (1:1) co-host system, similar EQE_{max} values were observed—30.3% at 10 wt% sensitizer and 28.1% at 12.5 wt% sensitizer, both with 1 wt% ***v*-DABNA**. However, a significant improvement to device efficiency roll-off was observed: the device with 10 wt% sensitizer and 1 wt% TE showed a 15.7% reduction in efficiency roll-off compared to the equivalent CzSi-hosted HP-OLED.

While most studies have focused on the standard PSF strategy, Chung et al. explored a new approach to hyperphosphorescence. Their deep-blue OLEDs employed the iridium(III)

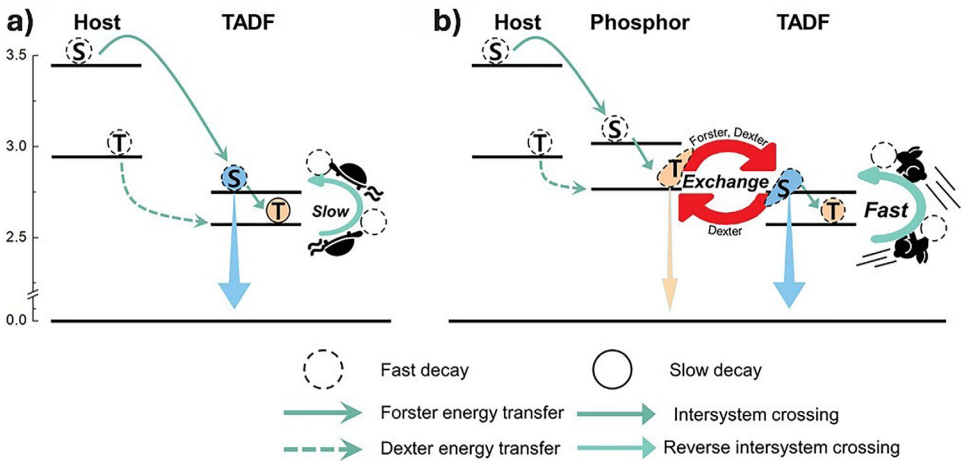

Figure 8. The emission mechanism of a) conventional TADF and b) EPHTADF devices. Reproduced with permission.[88] Copyright 2021, John Wiley and Sons.

complex **CN-Ir** as the sensitizer paired with the MR-TADF emitter ***ν*-DABNA** (Figure 6).[88] **CN-Ir** was selected to enable what the authors termed an energy-exchanging phosphorescence and TADF (EPHTADF) mechanism, an approach illustrated in **Figure 8**. This mechanism relies on the alignment of the energy levels of the host, the sensitizer and the TE to enable the simultaneous forward and backward energy transfer between the sensitizer and the TE. This provides a competitive exciton recycling pathway in lieu of an unproductive ISC on the MR-TADF TE, thereby reducing the triplet exciton population on the latter. As the back energy transfer allows for coemission from the sensitizer and the TE, careful management of the phosphor's photophysical properties is essential to suppress this undesired radiative process that would adversely affect the color purity of the device. By dynamically sharing excitons between the sensitizer and the TE, the EPHTADF mechanism significantly enhanced exciton utilization efficiency, leading to improved device EQE. Indeed, their devices showed an EQE_{max} of 27.3% and a remarkable operational lifetime, reflected in the LT_{50} exceeding 30 000 h at 100 cd m^{-2}. The device configuration contained 20 wt% **CN-Ir** and 0.5 wt% ***ν*-DABNA**, while higher doping concentrations of ***ν*-DABNA** resulted in a decreased device lifetime. Transient EL measurements revealed a marked difference in exciton dynamics between these devices. In Device B, which employed the putative EPHTADF mechanism, there was a rapid disappearance of triplet excitons, indicative of efficient exciton recycling and reduced triplet accumulation. In contrast, Device A, containing only ***ν*-DABNA**, exhibited slower exciton decay. The inclusion of **CN-Ir** in Device B also reduced the HOMO/LUMO gap between the host and the emitters, lowering the turn-on voltage to 3.0 V, compared to the 4.5 V required for the ***ν*-DABNA**-only Device A. This reflected the more facile charge injection in the former, contributing to its superior performance. Across the entire luminance range, Device B outperformed Device A, achieving an EQE_{max} of 27.3% versus 19.5% for Device A, while the efficiency roll-off was significantly reduced in Device B, maintaining an EQE of 23.3% at 1000 cd m^{-2} compared to 12.8% for Device A. These results evidence how judicious alignment of the state energies of the sensitizer and the TE can lead to exceptional device performance in both efficiency and stability as a result from optimizing exciton management. Additionally, the authors reported a top-emitting HP-OLED, Device C; however, EQE values were not provided due to its non-Lambertian emission pattern. Nevertheless, the authors noted that Device C exhibited a remarkable lifetime of LT_{50} of 493 h at 1000 cd m^{-2}, particularly considering that its CIE_y-coordinate is below 0.1.

3.2. Green Emission

Similar design strategies to those used for blue devices have been applied to green HP OLEDs. In the pursuit of green OLEDs, Zhang et al. introduced the MR-TADF emitter **AZA-BN** (**Figure 9**).[56] This emitter was designed using the so-called hybridized multiresonance and charge transfer (HMCT) approach, which combines the color purity of an MR-TADF core with the enhanced charge transfer dynamics of a donor–acceptor motif. By incorporating an aza-fused structure into the MR-TADF core, the design strengthened the intramolecular charge transfer character, improving exciton utilization. The HMCT strategy balances narrowband emission and efficient charge transport kinetics within the emissive layer of the device. The HP device employed ***fac*-Ir(ppy)** (30 wt%) as the sensitizer and **AZA-BN** (6 wt%) as the TE. The HP-OLED emitted at 527 nm and showed narrowband emission (FWHM of 30 nm). The device EQE_{max} was 28.2% and it exhibited moderately large efficiency roll-off, with EQE values of 26.5% at 100 cd m^{-2} and 19.1% at 1000 cd m^{-2}. Additionally, the device showed a moderate stability, with a LT_{90} of 46.3 h at 2000 cd m^{-2}. Notably, the device contained an unusually high doping concentration of the TE (6 wt%).

Palanisamy et al. also investigated MR-TADF TEs for green OLEDs by incorporating curvilinear indolocarbazole (pIC) donor units within two emitters, **BpIC-DPA** and **BpIC-Cz**, aiming to produce rigid TEs, which they asserted would lead to higher device stability (Figure 9).[89] Peripheral *tert*-butyl diphenylamine and carbazole donor moieties were incorporated to fine-tune the optoelectronic properties through an HMCT approach. This structural design resulted in narrowband emission, with

Ir Sensitizers

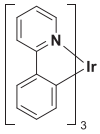

Ir(ppy)$_3$

Angew. Chem. Int. Ed. **2020**, *59*, 17499
Org. Electron. **2024**, *125*, 106973
Chem. Commun. **2024**, *60*, 6789
Angew. Chem. Int. Ed. **2023**, *62*, e202304104
Adv. Opt. Mater. **2025**, *14*, 2402131

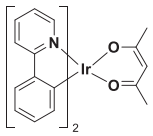

Ir(ppy)$_2$acac

J. Chem. Eng. **2024**, *481*, 148781

TADF Sensitizer

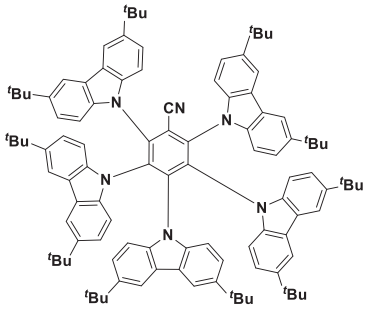

5tBuCzBN

Org. Electron. **2024**, *125*, 106973

Green MR-TADF TE

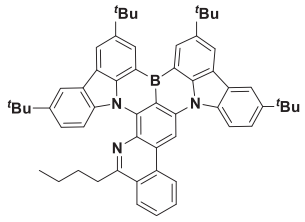

AZA-BN

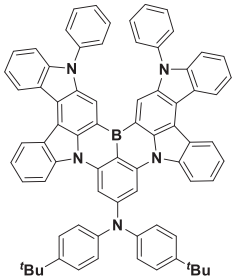

BpIC-DPA

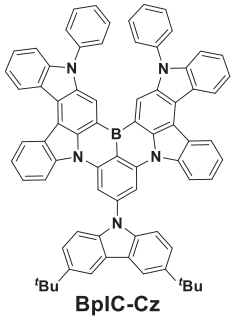

BpIC-Cz

Angew. Chem. Int. Ed. **2020**, *59*, 17499

J. Chem. Eng. **2024**, *481*, 148781

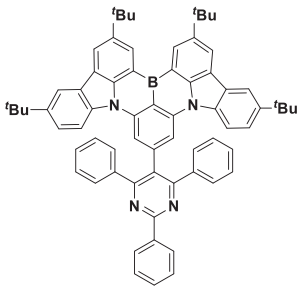

BN-TPP

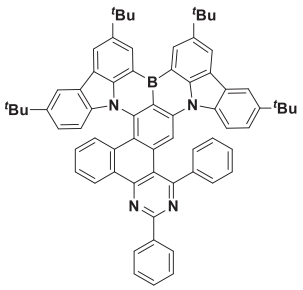

BN-DPBQ

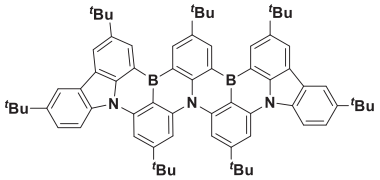

m-DBCz

Org. Electron. **2024**, *125*, 106973

Angew. Chem. Int. Ed. **2023**, *62*, e202304104

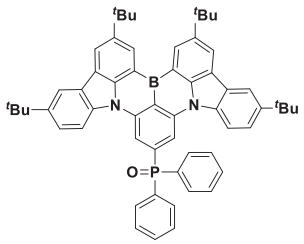

PhCzBN-PO

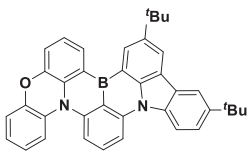

PXZ-tCzBN

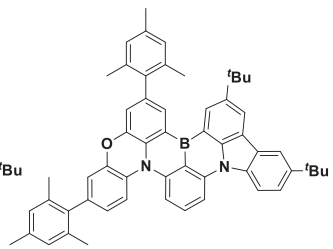

MesPXZ-tCzBN

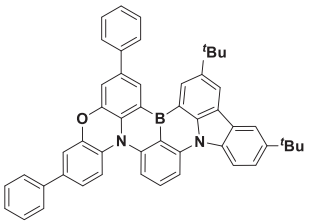

PhPXZ-tCzBN

Chem. Commun. **2024**, *60*, 6789

Adv. Opt. Mater. **2025**, *14*, 2402131

Figure 9. Structures of the Ir-based sensitizers and MR-TADF TEs employed in green HP-OLEDs.

emission maxima at 527 and 534 nm for 2 wt% **BpIC-DPA** and 4 wt% **BpIC-Cz** doped in DIC-TRZ, respectively, FWHM values below 25 nm, and PLQYs exceeding 83%. Efficient energy transfer was achieved in PSF films doped with a relatively low concentration (5 wt%) of the sensitizer **Ir(ppy)$_2$acac**. It is notable that efficient energy transfer was observed at such a low sensitizer loading, particularly when compared to studies such as that by Zhang et al.,[56] where higher sensitizer concentrations (e.g., 30 wt% **Ir(ppy)$_3$**) were employed to achieve excellent performance. The emission in these films originated from the TE and the lifetime of the delayed components were 11.12 and 11.74 µs for **BpIC-DPA** and **BpIC-Cz**, respectively, reduced from 31.9 and 34.4 µs for the respective MR-TADF emitter only films. HP-OLEDs with 2 wt% **BpIC-DPA** achieved an EQE$_{max}$ of 22.0%, with EQEs of 18.6 at 1000 cd m^{-2} and 16.2% at 5000 cd m^{-2}. Meanwhile, devices with 4 wt% **BpIC-Cz** performed even better, achieving an EQE$_{max}$ of 25.7%, with minimal efficiency roll off (EQE of 24.3% at 1000 cd m^{-2} and 22.6% at 5000 cd m^{-2}).

Song et al. explored strategies to modulate energy levels and excited-state lifetimes in MR-TADF materials. Their study focused on the emitters **BN-TPP** and **BN-DPBQ**, which they implemented in HP devices to achieve milder efficiency roll-off.[90] Both emitters contained a sterically bulky electron acceptor substituted onto the **DtCZB** core, producing **BN-TPP**, which was then further cyclized to form **BN-DPBQ** (Figure 9). The sensitizer–emitter combinations were optimized based on their spectral overlap integrals, with the TADF sensitizer **5tBuCzBN** (20 wt%) paired with **BN-TPP** (2 wt%) and the phosphorescent sensitizer ***fac*-Ir(ppy)$_3$** (8 wt%) paired with **BN-DPBQ** (2 wt%). PL spectra of the sensitized films confirmed efficient FRET in both cases. A notable observation was the stark contrast in delayed lifetimes. The sensitized films with **BN-TPP** showed a delayed lifetime of 1.4 µs, while those with **BN-DPBQ** exhibited 16.5 µs, representing both a much smaller reduction from its pristine value and an overall longer emission lifetime. This finding is surprising given the individual lifetimes of **BN-DPBQ** (30.6 µs) and ***fac*-Ir(ppy)$_3$** (1.6 µs)[91] compared to **BN-TPP** (67.2 µs) and **5tBuCzBN** (3.4 µs).[92]

Both HF and HP devices achieved improved EQE$_{max}$ and efficiency roll-off compared to their MR-TADF emitter-only analogs; however, the **BN-TPP**-sensitized device demonstrated superior performance, with an EQE$_{100}$ at 24.2% and EQE$_{1000}$ at 21.9%, compared to 20.8 and 16.3%, respectively, for the **BN-DPBQ**-sensitized device (Table 2). The stark contrast in concentration of the sensitizers—20 wt% for **5tBuCzBN** but only 8 wt% for ***fac*-Ir(ppy)$_3$** illustrates the importance of optimizing the concentrations of the sensitizer and TE combinations. This finding emphasizes the need for a more nuanced approach to sensitizer selection and device optimization, as achieving superior efficiency roll-off may require tailoring sensitizer properties beyond the spectral overlap with the TE.

Dong et al. introduced the green MR-TADF **PhCzBN-PO**, which incorporated of an electron-withdrawing diphenylphosphine oxide group onto the MR-TADF core (Figure 9).[93] The emitter was tested in devices at concentrations of 1 or 2 wt% on its own, as well as at 1 wt% with 20 wt% of the sensitizer ***fac*-Ir(ppy)$_3$**. In the HP-OLED configuration, the device achieved an impressive EQE$_{max}$ of 32.4%, significantly higher than the TE-only devices, which showed EQE$_{max}$ of 20.4 and 25.6% for the 1 and 2 wt% TE doping, respectively. Notably, while the TE-only devices experienced severe efficiency roll-off, with EQEs decreasing to 12.3% and 13.2%, respectively, at 1000 cd m^{-2}, the sensitized device with ***fac*-Ir(ppy)$_3$** showed much-improved efficiency roll-off, maintaining an EQE of 31.4% at this luminance. The EL FWHM also varied depending on the device configuration: the 1 wt% **PhCzBN-PO** device alone showed an FWHM of 26 nm, whereas the ***fac*-Ir(ppy)$_3$**-sensitized devices showed a slightly broader FWHM of 29 nm. This suggests some emission contribution from the sensitizer and inefficient FRET in the HP-OLED. Detailed device metrics are summarized in Table 2.

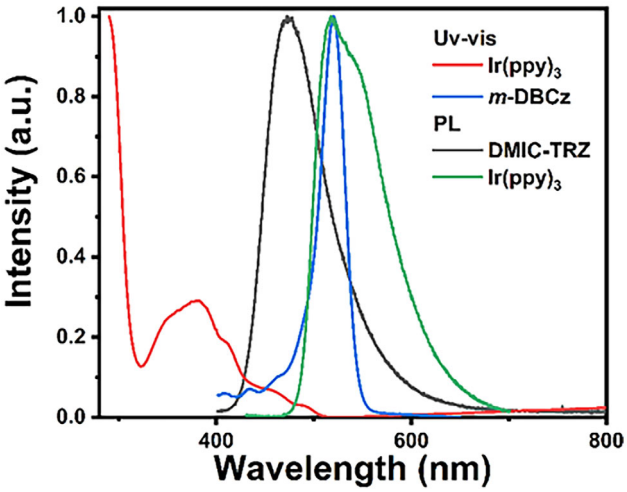

Figure 10. UV–vis absorption spectra of ***m*-DBCz** and ***fac*-Ir(ppy)$_3$** in toluene at a concentration of 10^{-5} M as well as PL spectra of 20 wt% ***fac*-Ir(ppy)$_3$**:DMIC-TRZ-doped film and DMIC-TRZ film. Reproduced with permission.[60] Copyright 2023, John Wiley and Sons.

Cai et al. employed an MR-TADF building block extension strategy, where azaboraanthracene moieties are assembled into a larger MR-TADF framework, ***m*-DBCz** (Figure 9).[60] This design led to a red-shifted emission, a shortened delayed fluorescence lifetime (14.8 µs), and a higher PLQY compared to the parent molecule, ***p*-TBNCz**. OLEDs employing ***m*-DBCz** alone achieved an impressive EQE$_{max}$ of 34.9%, which decreased to 31.3% at 1000 cd m^{-2}, 24.5% at 5000 cd m^{-2}, and 20.0% at 10 000 cd m^{-2}. Selecting ***fac*-Ir(ppy)$_3$** as the sensitizer (at 20 wt%) due it its strong spectral overlap with ***m*-DBCz**, as illustrated in **Figure 10**, and **DMIC-TRZ** as a TADF host material, produced films with an exceptionally short delayed lifetime of 385 ns.

The HP device demonstrated outstanding performance, achieving an EQE$_{max}$ of 36.3% with minimal efficiency roll-off, retaining EQEs of 35.1%, 34.2%, and 33.9% at 1000, 5000, and 10 000 cd m^{-2}, respectively. Even at an ultrahigh brightness of 100 000 cd m^{-2}, the device maintained an EQE of 27.7%, highlighting the effectiveness of the combination of the DMIC-TRZ host with a phosphorescent sensitizer. Device results using both **DMIC-TRZ** and a conventional fluorescent host material, **PhCzBCz** are summarized in Table 2.

Nemma et al. reported the development of π-extended phenoxazine-based asymmetric MR-TADF emitters, **PhPXZ-tCzBN** and **MesPXZ-tCzBN**, which feature a more π-conjugated structure compared to their parent **PXZ-tCzBN** (Figure 9),[35]

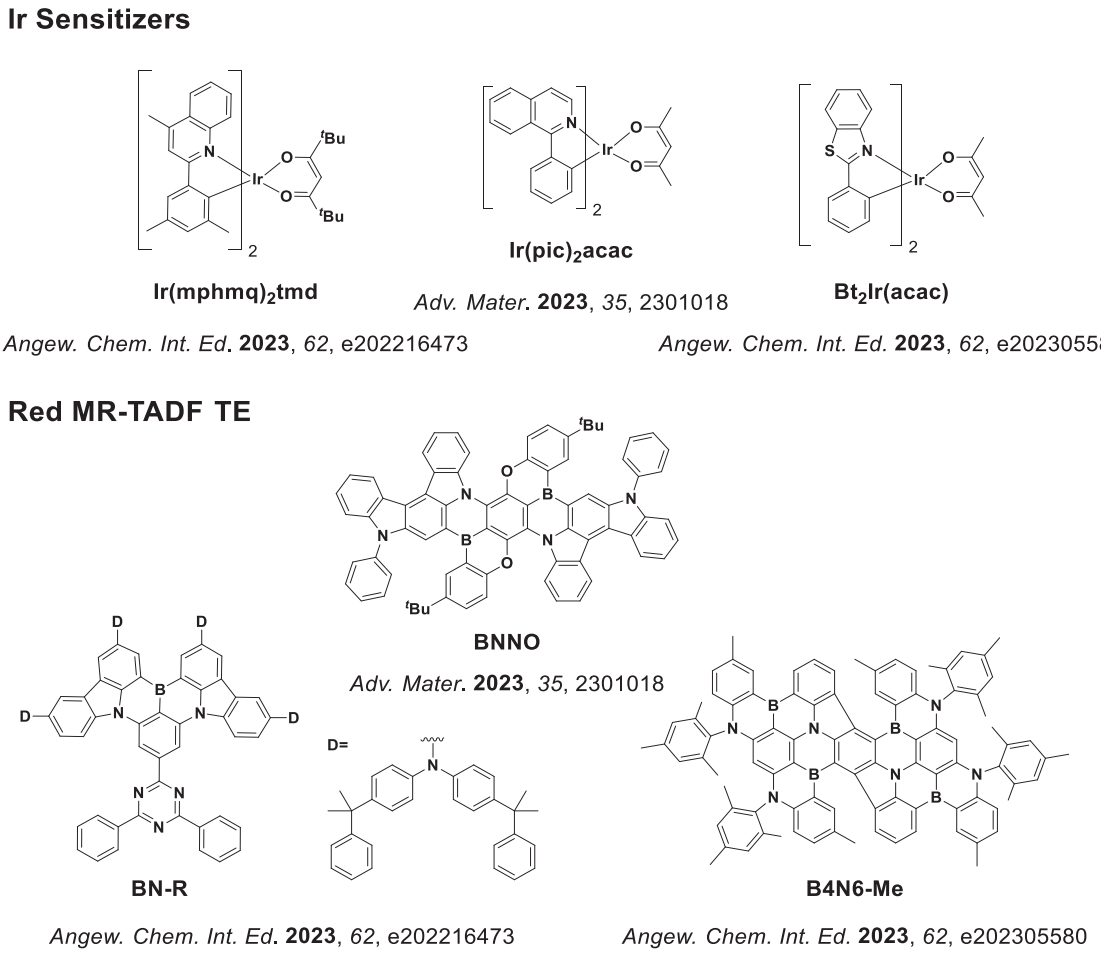

Figure 11. Structures of the Ir-based sensitizers and MR-TADF TEs employed in red HP-OLEDs.

designed to cause a red-shifted emission, thereby enhancing the spectral overlap integral with the sensitizer ***fac*-Ir(ppy)$_3$** to improve energy transfer. The PSF films, using 5 wt% TE and 20 wt% sensitizer, showed marginally lower PLQYs and slightly broader FWHM in all cases when compared to their TE-only films. This suggests that energy transfer is not fully efficient, while the significant reduction in excited-state lifetimes of the emitters (≈10 µs compared to ≈100 µs for the TE-only films) nonetheless indicates a strong contribution from FRET. In HP-OLEDs, the EQE$_{max}$ was 20.7% for the device using **PXZ-tCzBN** and 27.6% for both devices using **PhPXZ-tCzBN** and **MesPXZ-tCzBN**. Efficiency roll-off was minimal across all three devices, with EQE$_{1000}$ values of 18.8%, 25.7%, and 25.5% for **PXZ-tCzBN**, **PhPXZ-tCzBN**, and **MesPXZ-tCzBN**, respectively. The devices also demonstrated very low turn-on voltages of ≈2.2 V and maintained operation at 3 V even at a luminance of 1000 cd m^{-2}. Notably, the operational stability of the device with **PhPXZ-tCzBN** was particularly high, with the HP-OLED achieving an LT$_{95}$ of over 3000 h and an LT$_{90}$ over 8600 at 1000 cd m^{-2}.

Among the examples discussed, **Ir(ppy)$_3$** stands out as the sensitizer of choice for green HP-OLEDs. It has proven suitable for sensitizing a wide range of MR-TADF TEs and the resulting devices have shown particularly attractive performance metrics. However, while these studies do highlight the consistent effectiveness of **Ir(ppy)$_3$** as a sensitizer for HP-OLEDs, it is difficult to determine its specific contribution to device performance given the variability in hosts, TEs, and doping concentrations across these reported systems. Despite this, the remarkable color purity, efficiency, and stability achieved by these green-emitting systems illustrate the potential of HP-OLED technology.

3.3. Red Emission

Recent advances in red-emitting MR-TADF emitters have opened up the potential for their use in HP-OLEDs. Relative to blue and green HP devices, red-emissive HP-OLEDs have been far less explored. Cai et al. reported a solution-processable red MR-TADF emitter, **BN-R**, designed to address the challenges of low efficiency and color purity in red OLEDs (**Figure 11**).[58] By modifying a boron–nitrogen-containing MR-TADF framework with auxiliary donor and acceptor groups, the emission was red-shifted to 624 nm (FWHM of 46 nm) yet remained bright (PLQY of 94% in toluene) and narrowband compared to the parent

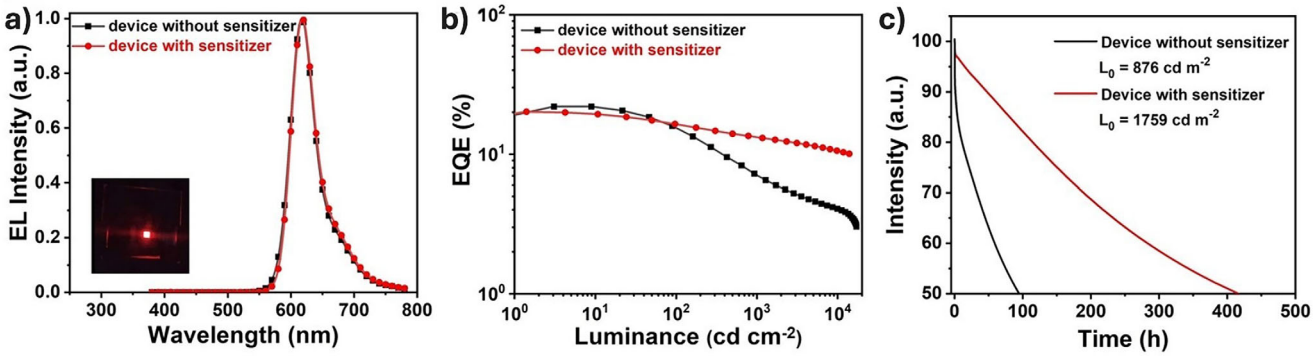

Figure 12. a) EL spectra and b) EQE-L curves of devices with and without sensitizer using 1 wt% doping of **BN-R** as the TE. c) The lifetime of devices with and without sensitizer based on **BN-R** with 1 wt% doping concentration at an initial current density of 10 mAcm^{-2}. Adapted with permission.[58] Copyright 2023, John Wiley and Sons.

emitter. **BN-R** was used in HP devices partnered with the sensitizer **Ir(mphmq)$_2$tmd**. At 3 wt% **Ir(mphmq)$_2$tmd** and 1 wt% **BN-R**, PSF films produced emission exclusively from **BN-R**, with a PLQY of 95% and a delayed lifetime of 9 µs, reduced from 71.9 µs when there is no sensitizer (**Figure 12a**). The resulting HP-OLEDs showed an EQE$_{max}$ of 20.1%, had moderate efficiency roll-off with EQE$_{100}$ 16.4% and EQE$_{1000}$ 13.3% (Figure 12b). While the EQE$_{max}$ was slightly lower compared to the devices without the sensitizer (22.0%), the HP device demonstrated a significantly longer operational lifetime, with an LT$_{50}$ increasing from 94.7 to 416.7 h (Figure 12c). Device metrics for the HP device are summarized in Table 2.

The devices used a relatively low sensitizer doping concentration (3 wt%) compared to other high-performing PSF systems. Furthermore, the authors noted that **BN-R** likely exhibits preferential horizontal alignment of its transition dipole moment, which, when combined with its high PLQY, highlights the potential for further optimization of the device EQE to reach its theoretical maximum efficiency.

Fan et al. introduced **BNNO**, a high-efficiency narrowband red-emitting MR-TADF emitter designed to deliver exceptional color purity and stability in vacuum-deposited devices (Figure 11).[94] **BNNO** consists of fused indolocarbazole moieties in a boron/oxygen-embedded skeleton, and is notable as the first red MR-TADF emitter to meet the BT.2020 red point of (0.708, 0.292). **BNNO** emits at 637 nm (FWHM of 32 nm) and has a PLQY of 95% in toluene. The HP-OLEDs employed **Ir(piq)$_2$acac** as the sensitizer due to its significant spectral overlap with the absorption spectrum of **BNNO**. The PSF films showed an intense emission from **BNNO**, with a PLQY of 97%. Devices with 8 wt% **Ir(piq)$_2$acac** and 1 wt% **BNNO** showed an EQE$_{max}$ of 34.4%, and only modest efficiency roll-off (EQE$_{1000}$ of 31.4% and EQE$_{10000}$ of 24.6%). In contrast, the reference device using **Ir(piq)$_2$acac** alone achieved a significantly lower EQE$_{max}$ of 19.5%. The high EQE observed in **BNNO**-sensitized devices was attributed to the strongly preferential horizontal orientation of the emitting dipoles. Furthermore, the HP devices exhibited exceptional stability, with an extrapolated LT$_{95}$ exceeding 10 000 h at 1000 cd m^{-2}, far surpassing typical operational benchmarks for red OLEDs. These findings highlight **BNNO**'s remarkable stability, efficiency, and color purity, cementing its position as a leading TE for red HP-OLEDs. Device results are detailed in Table 2.

Fan et al. introduced the MR-TADF emitter **B4N6-Me**, designed to produce narrowband orange-red emission (Figure 11).[57] The emitter contains four boron atoms and six nitrogen atoms arranged in *para* B–π–N and B–π–B/N–π–N patterns. This design balances the narrowband emission characteristics of the *para* B–π–N motif with the spectral red-shift introduced by the B–π–B/N–π–N configuration. The resulting compound emits at λ_{max} 580 nm, has a small FWHM of only 19 nm (70 meV) in toluene and has a high PLQY of 98%.

Bt$_2$Ir(acac) was chosen as the sensitizer at 10 wt%, given significant spectral overlap with the absorption spectrum of **B4N6-Me**. This overlap enables efficient energy transfer, although evidence of incomplete FRET was observed in the EL spectra, as shown by a minor shoulder attributed to **Bt$_2$Ir(acac)**. Despite this, the HP devices achieved outstanding EQE$_{max}$ exceeding 34% when **B4N6-Me** was used at concentrations of 1–2 wt%. At higher luminance levels, the efficiency roll-off behavior was strongly influenced by the TE concentration; increased DET to **B4N6-Me** caused aggregation-induced triplet–triplet quenching, negatively impacting performance. Optimized devices with 1 wt% **B4N6-Me** achieved a remarkable EQE$_{max}$ of 35.8% with moderate efficiency roll-off (EQE$_{1000}$ of 28.4%). In contrast, control devices using only **B4N6-Me** reached a comparable EQE$_{max}$ of 31.7% but suffered from much more severe efficiency roll-off, with an EQE$_{1000}$ of just 11.2%. This comparison highlights the effectiveness of the HP approach in mitigating efficiency roll-off. Notably, the performance of the devices was in part attributed to the formation of an interfacial exciplex between PO-T2T and DMIC-TRZ, which facilitated RISC. This exemplifies the synergistic interplay between the device architecture, as well as the choice of host, and the device performance. Detailed device metrics are summarized in Table 2.

These studies collectively illustrate how high-performance red and orange-red devices can be obtained when combining finely tuned MR-TADF emitters with suitable phosphorescent sensitizers, including examples that meet the BT.2020 standard for red.

4. Organic Sensitizers

The growing desire to use sustainable materials has prompted significant interest in organic sensitizers, including those

Table 3. Key device performance characteristics of hyperphosphorescent OLEDs with organic sensitizers and MR-TADF emitters.

Sensitizer (S)	Terminal emitter (TE)	Composition of emissive layer	Turn-on [V]	EQE_{max} [%]	EQE_{100} [a] [%]	EQE_{1000} [b] [%]	$CIE_{x,y}$	λ_{max} [nm]
3,2-PIC-TXT	BN2	mCPBC:S (20 wt%):TE (1 wt%)	2.8	43.8	–	21.6	0.32, 0.65	540
3,2-PIC-TXT	tCzphB-Fl	mCPBC:S (20 wt%):TE (2 wt%)	2.8	43.3	–	28.3	0.29, 0.68	538
3,2-PIC-TXT	tCzphB-Ph	mCPBC:S (20 wt%):TE (2 wt%)	2.8	40.9	–	28.0	0.23, 0.71	526
3,2-PIC-XT	BN2	mCPBC:S (20 wt%):TE (1 wt%)	2.8	41.9	–	20.9	0.32, 0.65	540
3,2-PIC-XT	tCzphB-Fl	mCPBC:S (20 wt%):TE (2 wt%)	2.8	40.6	–	29.3	0.29, 0.67	538
3,2-PIC-XT	tCzphB-Ph	mCPBC:S (20 wt%):TE (2 wt%)	2.8	38.0	–	27.5	0.22, 0.71	526
$Ir(ppy)_3$ [c]	BN2	mCPBC:S (10 wt%):TE (1 wt%)	3.2	37.0	–	26.7	0.33, 0.65	544
$Ir(ppy)_3$ [c]	tCzphB-Fl	mCPBC:S (10 wt%):TE (2 wt%)	3.3	37.7	–	30.2	0.29. 0.68	538
$Ir(ppy)_3$ [c]	tCzphB-Ph	mCPBC:S (10 wt%):TE (2 wt%)	3.2	38.0	–	30.8	0.23, 0.72	528
RTP-D2	S-Cz-BN	S:TE (2 wt%)	2.7	26.4	–	18.1	0.12, 0.45	–
RTP-D3	DtBuCzB	S:TE (3 wt%)	2.7	19.4	–	6.0	0.11, 0.47	–
RTP-D3	tCzphB-Ph	S:TE (2 wt%)	2.8	24.6	–	8.2	0.25, 0.70	–
RTP-D3	BNO1	S:TE (1 wt%)	3.4	6.8	–	1.9	0.58, 0.35	–

[a] External quantum efficiency at 100 cd m^{-2}; [b] External quantum efficiency at 1000 cd m^{-2}; [c] Heavy metal sensitizer, included for comparison.

exhibiting room-temperature phosphorescence (RTP). While numerous organic RTP materials have been reported in the literature, their application in OLEDs has faced significant challenges. One of the main obstacles is the long phosphorescence lifetimes typical of these materials. Additionally, factors such as weak spin–orbit coupling, exciton quenching, and low PLQY complicate the development of high-performance RTP materials and often result in poor device performance.[95]

Despite these challenges, recent studies have demonstrated the potential of organic phosphorescent materials to serve as effective sensitizers in HP-OLEDs (**Table 3**). Zeng et al. reported the compounds **3,2-PIC-XT**[96] and **3,2-PIC-TXT**[97] that can function remarkably well as sensitizers for the green MR-TADF terminal emitters **BN2**, **tCzphB-Ph**, and **tCzphB-Fl** (**Figure 13**). The absorption spectra of the three TEs overlap well with the PL spectra of **3,2-PIC-XT** and **3,2-PIC-TXT**, enabling efficient FRET. HP-OLEDs were optimized using 1 wt% **BN2**, 2 wt% **tCzphB-Ph**, and 2 wt% **tCzphB-Fl**, in combination with 20 wt% of the RTP sensitizers. For direct comparison, HP-OLEDs with the phosphorescent emitter ***fac*-Ir(ppy)$_3$** at 10 wt% were also fabricated.

EL emission from **3,2-PIC-XT** and **3,2-PIC-TXT** was virtually undetectable in the HP-OLEDs, implying complete energy transfer from the RTP sensitizers to the MR-TADF TEs. The resulting devices achieved outstanding EQE_{max} values ranging from 38.0% to 41.9%, surpassing those of devices with ***fac*-Ir(ppy)$_3$** (which exhibited EQE_{max} of 37.0% to 38.0%). Despite these high EQE values, the devices sensitized by the RTP emitters exhibited efficiency roll-off values of ≈25% to 50% at EQE_{1000}, higher than those with ***fac*-Ir(ppy)$_3$** devices, which showed efficiency roll-off in the region of 20%. To address this, an interlayer sensitization strategy was implemented, in which the TE emitting layer was sandwiched in between two thin sensitization layers to reduce DET. The resulting devices demonstrated much higher EQEs at 1000 cd m^{-2}, suggesting a useful device stack strategy to mitigate efficiency roll-off.

Xu et al. designed the donor–oxygen–acceptor (DOA) organic phosphor, **RTP-D2**, which demonstrated intriguing aggregation-induced organic room-temperature electrophosphorescence (Figure 13).[98] This aggregation-induced emission enabled host-free sensitization of MR-TADF emitters, simplifying the device architecture and eliminating the need for a wide bandgap host material. **S-Cz-BN** (Figure 13) was selected as the TE due to its favorable spectral overlap with **RTP-D2** and its lower T_1 energy, which facilitated efficient FRET from **S-Cz-BN** to **RTP-D2**. The doping level of **S-Cz-BN** was set to 2 wt% to suppress DET. The EL spectrum of the resulting HP-OLED was much sharper than in the device using **RTP-D2** alone, with an FWHM of 26 nm, down from 99 nm. The EQE_{max} of the HP-OLED was also improved, achieving 26.4% (and EQE_{1000} = 18.1%) compared to the nonsensitized device, which showed EQE_{max} of 15.8% and EQE_{1000} of 11.7%.

Xu and co-workers explored other DOA organic phosphors, including **RTP-D3**, a weakly emissive RTP compound that challenges the conventional idea that the best sensitizers should also be high PLQY emitters (Figure 13).[99] By replacing the acridine donor for a carbazole, **RTP-D3** exhibited a low aggregation-induced RTP PLQY of 12.8%, in contrast to the 77.5% PLQY recorded for **RTP-D2**. Despite this much lower PLQY, **RTP-D3** was used in sensitized host-free HP-OLEDs, fabricated with 2 wt% **tCzphB-Ph** as the TE (Figure 13). The optimized device architecture showed an EQE_{max} of 24.6%, although severe efficiency roll-off was observed, with EQE_{1000} dropping to 8.2%. Further applications of **RTP-D3** were explored in HP-OLEDs with the blue-emitting **D*t*BuCzB** and red-emitting **BNO1** compounds as TEs (Figure 13), achieving EQE_{max} of 19.4% and 6.8%, respectively. These results demonstrate the versatility of this weakly emissive RTP compound as a sensitizer.

These examples demonstrate the growing potential of purely organic phosphorescent RTP materials as sensitizers in HP-OLEDs. As interest in RTP continues to increase, it is expected that HP-OLEDs sensitized by these materials will see further advancements, driving the development of more efficient, sustainable OLED technologies.

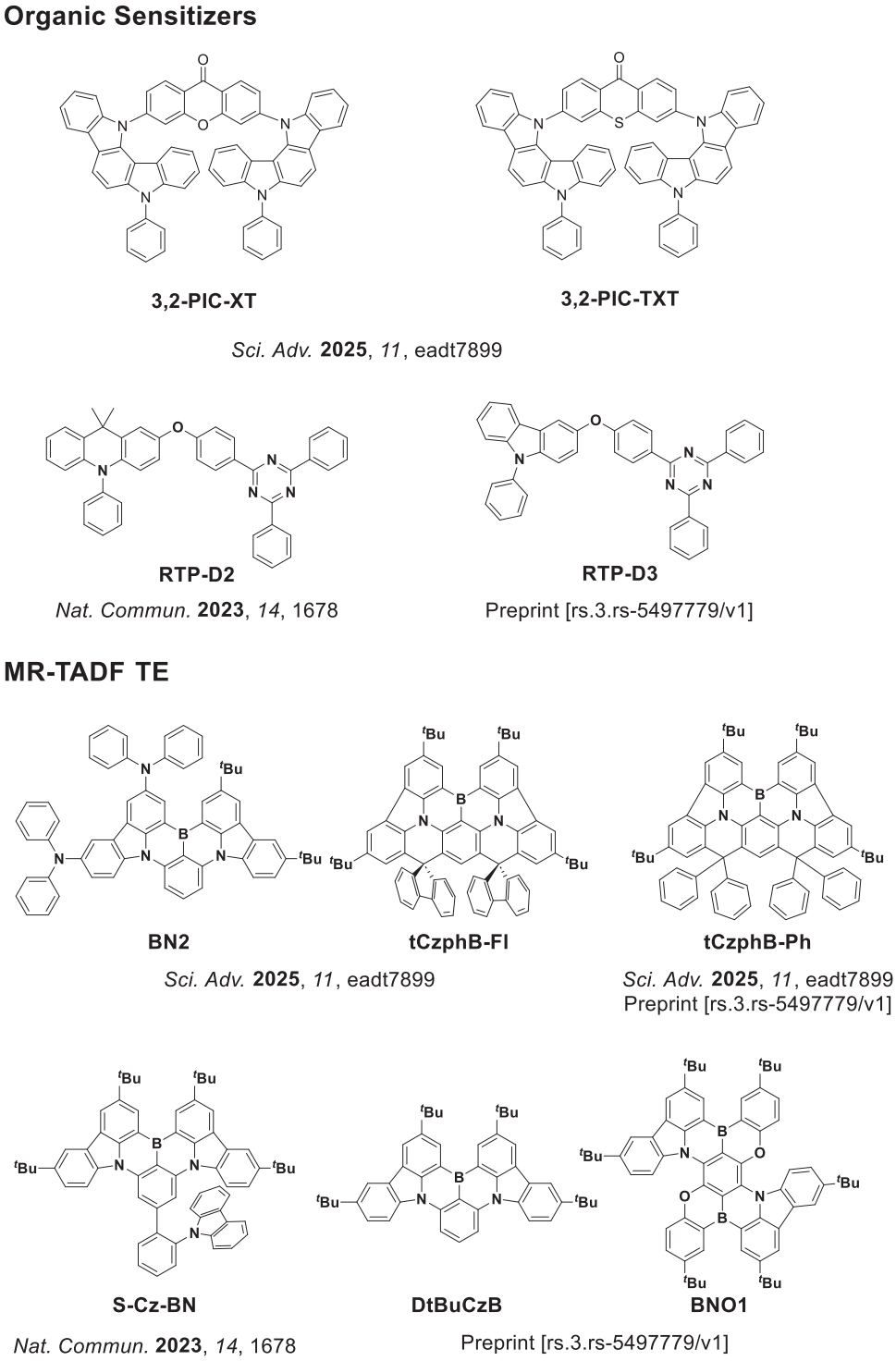

Figure 13. Structures of the organic sensitizers and MR-TADF TEs employed in HP-OLEDs.

5. Conclusions

This review highlights the transformative potential of pairing MR-TADF emitters with phosphorescent Pt and Ir sensitizers, as well as emerging organic RTP sensitizers, in HP-OLEDs. Significant progress has been made in optimizing energy transfer processes, materials design, and device architectures, resulting in improved efficiencies, color purity, and operational lifetimes in devices emitting across the visible spectrum and beyond.

Key trends reveal that high FRET efficiency remains central to achieving high exciton utilization efficiency and minimizing degradation pathways, such as TTA. Efficient FRET relies on a

strong spectral overlap between the emission of the sensitizer and the absorption of the TE. Greater spectral overlap not only improves energy transfer efficiency but also extends the Förster radius, enabling exciton transfer over larger distances. This is particularly beneficial in reducing exciton losses due to quenching. Selecting sensitizers to avoid long, low-energy emission tails is critical to maximizing these benefits. Advances in MR-TADF molecular design, such as incorporating sterically bulky groups and rigid frameworks, contribute to reducing undesired excimer formation as well as DET and improving device stability and color purity. These strategies have also shown success in platinum- and iridium-based sensitizers. Prioritizing FRET over DET in HP devices leads to reduced efficiency roll-off in the device that also translates into more stable devices.

Another critical consideration is the role of sensitizer or TE concentration in optimizing energy transfer efficiency. Higher doping concentrations can enhance FRET by enabling closer proximity between donor and acceptor molecules, ultimately leading to improved exciton utilization and overall device efficiency. However, this requires careful molecular design to prevent quenching effects, such as aggregation or excimer formation, which can offset these benefits. While some systems have shown efficient energy transfer at high doping concentrations, many high-performing HP-OLEDs have benefitted from lower doping levels of the TE that strike a balance between energy transfer efficiency and minimal quenching.

Both Pt- and Ir-based sensitizers have been shown to work effectively in HP-OLEDs, with examples available across a range of emission colors. Recently, organic RTP materials have emerged as a promising class of sensitizers, offering a more sustainable alternative to organometallic phosphors, and expanding the range of materials available for HP-OLEDs. Of the examples surveyed, Ir-based sensitizers tend to produce HP-OLEDs showing higher external quantum efficiencies and reduced efficiency roll-off. Among the MR-TADF TEs, ***ν*-DABNA** has been used prominently in both HF- and HP-OLEDs, and has been shown to work compatibly with a large number of Pt and Ir sensitizers. These HP devices consistently show EQE_{max} above 20%, with many examples exceeding 30%, and display moderate roll-off. ***ν*-DABNA** offers a combination of narrowband emission, fast k_{RISC}, high PLQY, and strong absorption, all of which are desirable in a TE.

A particularly promising approach that has emerged is the development of materials and device designs that enable efficient recycling of triplet excitons to form radiative singlets on the TE. HMCT designs have been shown to facilitate RISC in MR-TADF emitters, providing a route to improved triplet exciton recycling in HP-OLEDs. While HMCT-based TEs have demonstrated promising performance in HP-OLEDs, with high EQEs and reduced efficiency roll off in some cases, systematic studies comparing HMCT and non-HMCT TEs are lacking, making it difficult to attribute these improvements in device performance solely to exciton recycling. Similarly, EPHTADF (Energy-Exchanging Phosphorescence and TADF) systems offer an alternative exciton management strategy, dynamically recycling excitons between the sensitizer and MR-TADF TE to reduce triplet accumulation and enhance operational stability.

While significant advances have been made, further progress in PSF systems will require careful consideration of several interrelated factors. In many of the studies discussed, TE concentrations are optimized to achieve efficient FRET, as indicated by the absence of sensitizer emission. However, apparent FRET efficiency does not necessarily equate to absolute exciton harvesting efficiency, as alternative pathways such as DET followed by upconversion (or indeed, non-radiative decay) may contribute to hidden exciton pathways. Focusing predominantly on optimizing the TE concentration may also overlook opportunities to enhance energy transfer dynamics and device performance. Since sensitizers too play a critical role in determining FRET efficiency and exciton dynamics, tailoring sensitizer concentrations alongside TE concentrations could unlock further improvements in efficiency, stability, and efficiency roll-off behavior. Future research should consider not only optimizing FRET efficiency but also systematically investigating hidden loss channels, ensuring that energy transfer mechanisms are fully understood and leveraged to maximize device performance. The use of organic RTP materials as sensitizers presents a promising direction for more sustainable HP-OLEDs, though challenges remain, such as efficiency roll-off at high luminance. Nonetheless, recent strategies such as interlayer sensitization and host-free RTP systems have demonstrated significant potential in overcoming these obstacles.

To optimize HP-OLED performance the following considerations are required.

1) Spectral overlap to induce efficient FRET: Prioritize a strong overlap between the emission spectrum of the phosphorescent sensitizer and the absorption spectrum of the MR-TADF emitter. This maximizes FRET efficiency and increases the Förster radius, critical for effective energy transfer.
2) Sensitizer–emitter pairing to target specific emission color: Tailor the combination of sensitizers and emitters to ensure optimal energy transfer dynamics and narrowband emission uniquely from the TE, avoiding emission tails in the sensitizer that fall below the emitter's absorption range and minimizing non-radiative losses.
3) Sterically bulky substituents on the sensitizer and/or TE: The strategic incorporation of sterically bulky substituents not only mitigates aggregation and excimer formation but also suppresses undesired DET, especially when the sensitizer and/or TE is used at relatively high doping concentrations.
4) Optimized doping concentrations: Carefully balancing the doping levels of the sensitizers and the TE is needed not only to ensure efficient FRET but also to control concentration quenching and, in some cases, charge transfer kinetics within the emissive layer.
5) Exciton management: Building in pathways for triplet excitons to be rapidly converted into radiative singlets on the TE, either through RISC on the TE or via FRET to the host or sensitizer may lead to more efficient and stable devices.

These five factors are closely interconnected, requiring materials and device optimization such that not only are the properties of each of the sensitizer and TE fine-tuned, but that their photophysics is suitably matched to permit effective energy transfer. The examples surveyed here are a testament to the potential of HP-OLEDs to deliver long-coveted efficient and stable devices.

Acknowledgements

E.V.P. was funded by the European Union from its Framework Programme for Research and Innovation Horizon Europe (2021–2027), under the Marie Sklodowska-Curie Grant Agreement No. 101108406. E.Z.-C. thanks the Engineering and Physical Sciences Research Council of the UK (Grant Nos. EP/W007517/1, EP/W015137/1, and EP/Z535291/1) for support, and the authors acknowledge support from JSPS Core-to-Core Program (Grant No. JPJSCCA20220004). Views and opinions expressed are those of the author only and do not necessarily reflect those of the European Union or the European Research Executive Agency (granting authority). Neither the European Union nor the granting authority can be held responsible for them. We thank André Jung and Jasmin Seibert for their contributions to organizing and reviewing the literature.

Open access funding enabled and organized by Projekt DEAL.

Conflict of Interest

The authors declare no conflict of interest.

Keywords

device stability, external quantum efficiency (EQE), Förster resonance energy transfer (FRET), hyperphosphorescence (HP), multiresonance thermally activated delayed fluorescence (MR-TADF), organic light-emitting diodes (OLEDs), phosphor-sensitized fluorescence (PSF)

Received: February 14, 2025
Revised: April 16, 2025
Published online:

[1] S.-J. Zou, Y. Shen, F.-M. Xie, J.-D. Chen, Y.-Q. Li, J.-X. Tang, *Mater. Chem. Front.* **2020**, *4*, 788.
[2] G. Hong, X. Gan, C. Leonhardt, Z. Zhang, J. Seibert, J. M. Busch, S. Brase, *Adv. Mater.* **2021**, *33*, 2005630.
[3] S. Sudheendran Swayamprabha, D. K. Dubey, Shahnawaz, R. A. K. Yadav, M. R. Nagar, A. Sharma, F.-C. Tung, J.-H. Jou, *Adv. Sci.* **2021**, *8*, 2002254.
[4] S. M. K. A. Naqvi, M. F. Baig, T. Farid, Z. Nazir, S. A. H. Mohsan, Z. Liu, W. Cai, S. Chang, *Nanomaterials* **2023**, *13*, 3020.
[5] J. M. dos Santos, D. Hall, B. Basumatary, M. Bryden, D. Chen, P. Choudhary, T. Comerford, E. Crovini, A. Danos, J. De, S. Diesing, M. Fatahi, M. Griffin, A. K. Gupta, H. Hafeez, L. Hämmerling, E. Hanover, J. Haug, T. Heil, D. Karthik, S. Kumar, O. Lee, H. Li, F. Lucas, C. F. R. Mackenzie, A. Mariko, T. Matulaitis, F. Millward, Y. Olivier, Q. Qi, et al., *Chem. Rev.* **2024**, *124*, 13736.
[6] J. H. Kwon, *Front. Chem.* **2024**, *12*, 1441517.
[7] P. L. dos Santos, P. Stachelek, Y. Takeda, P. Pander, *Mater. Chem. Front.* **2024**, *8*, 1731.
[8] E. Tankelevičiūtė, I. D. W. Samuel, E. Zysman-Colman, *J. Phys. Chem. Lett.* **2024**, *15*, 1034.
[9] M. Y. Wong, E. Zysman-Colman, *Adv. Mater.* **2017**, *29*, 1605444.
[10] M. Godumala, S. Choi, M. J. Cho, D. H. Choi, *J. Mater. Chem. C* **2019**, *7*, 2172.
[11] E. V. Puttock, C. S. K. Ranasinghe, M. Babazadeh, J. Jang, D. M. Huang, Y. Tsuchiya, C. Adachi, P. L. Burn, P. E. Shaw, *Macromolecules* **2020**, *53*, 10375.
[12] P. Pander, Y. M. Dikova, E. V. Puttock, J. A. G. Williams, *Inorg. Chem. Front.* **2024**, *11*, 7545.
[13] H.-T. Mao, G.-F. Li, G.-G. Shan, X.-L. Wang, Z.-M. Su, *Coord. Chem. Rev.* **2020**, *413*, 213283.
[14] Q. Wei, N. Fei, A. Islam, T. Lei, L. Hong, R. Peng, X. Fan, L. Chen, P. Gao, Z. Ge, *Adv. Opt. Mater.* **2018**, *6*, 1800512.
[15] A. Thamarappalli, C. S. K. Ranasinghe, J. Jang, M. Gao, P. L. Burn, E. V. Puttock, P. E. Shaw, *Adv. Funct. Mater.* **2022**, *32*, 2205077.
[16] F. Maasoumi, R. D. Jansen-van Vuuren, P. E. Shaw, E. V. Puttock, R. C. R. Nagiri, J. A. McEwan, M. Bown, J. L. O'Connell, C. J. Dunn, P. L. Burn, E. B. Namdas, *npj Flexible Electron.* **2018**, *2*, 27.
[17] M. A. Baldo, D. F. O'Brien, Y. You, A. Shoustikov, S. Sibley, M. E. Thompson, S. R. Forrest, *Nature* **1998**, *395*, 151.
[18] R. Ansari, W. Shao, S.-J. Yoon, J. Kim, J. Kieffer, *ACS Appl. Mater. Interfaces* **2021**, *13*, 28529.
[19] H. Lee, B. Park, G. R. Han, M. S. Mun, S. Kang, W. P. Hong, H. Y. Oh, T. Kim, *Adv. Mater.* **2024**, *36*, 2409394.
[20] C. Murawski, K. Leo, M. C. Gather, *Adv. Mater.* **2013**, *25*, 6801.
[21] J. Kalinowski, J. Mężyk, F. Meinardi, R. Tubino, M. Cocchi, D. Virgili, *J. Appl. Phys.* **2005**, *98*, 063532.
[22] S. Kang, J. Y. Lee, T. Kim, *Electron. Mater. Lett.* **2020**, *16*, 1.
[23] P. Santhoshini, K. HelenPrabha, *J. Comput. Electron.* **2024**, *23*, 977.
[24] J. Yan, D.-Y. Zhou, L.-S. Liao, M. Kuhn, X. Zhou, S.-M. Yiu, Y. Chi, *Nat. Commun.* **2023**, *14*, 6419.
[25] K. Stavrou, L. G. Franca, A. Danos, A. P. Monkman, *Nat. Photonics* **2024**, *18*, 554.
[26] L. Paterson, A. Mondal, P. Heimel, R. Lovrincic, F. May, C. Lennartz, D. Andrienko, *Adv. Electron. Mater.* **2019**, *5*, 1900646.
[27] H. Nakanotani, T. Higuchi, T. Furukawa, K. Masui, K. Morimoto, M. Numata, H. Tanaka, Y. Sagara, T. Yasuda, C. Adachi, *Nat. Commun.* **2014**, *5*, 4016.
[28] Y. Gawale, R. Ansari, K. R. Naveen, J. H. Kwon, *Front. Chem.* **2023**, *11*, 1211345.
[29] U. Deori, G. P. Nanda, C. Murawski, P. Rajamalli, *Chem. Sci.* **2024**, *15*, 17739.
[30] S. K. Behera, R. D. Costa, *J. Mater. Chem. C* **2023**, *11*, 13647.
[31] M. A. Baldo, M. E. Thompson, S. R. Forrest, *Nature* **2000**, *403*, 750.
[32] T. Förster, *Ann. Phys.* **1948**, *437*, 55.
[33] B. Sk, S. Hirata, *Chem. Commun.* **2023**, *59*, 6643.
[34] S. Nam, J. W. Kim, H. J. Bae, Y. M. Maruyama, D. Jeong, J. Kim, J. S. Kim, W.-J. Son, H. Jeong, J. Lee, S.-G. Ihn, H. Choi, *Adv. Sci.* **2021**, *8*, 2100586.
[35] H. Nemma, Y. Kori, N. Meguro, R. Mimura, Y. Chiba, J. Kido, H. Sasabe, *Adv. Opt. Mater.* **2025**, *13*, 2402131.
[36] T. Baumann, M. Budzynski, C. Kasparek, *Dig. Tech. Pap. – SID Int. Symp.* **2019**, *50*, 466.
[37] N. Haase, A. Danos, C. Pflumm, P. Stachelek, W. Brutting, A. P. Monkman, *Mater. Horiz.* **2021**, *8*, 1805.
[38] Y. Wu, M. Huang, L. Cheng, J. Zhang, Y. Pan, S.-M. Yiu, K. C. Lau, J. Yan, C. Yang, Y. Chi, *Angew. Chem., Int. Ed.* **2025**, *64*, 202421664.
[39] S. H. Han, J. H. Jeong, J. W. Yoo, J. Y. Lee, *J. Mater. Chem. C* **2019**, *7*, 3082.
[40] W. Xie, X. Peng, M. Li, W. Qiu, W. Li, Q. Gu, Y. Jiao, Z. Chen, Y. Gan, K. k. Liu, S. J. Su, *Adv. Opt. Mater.* **2022**, *10*, 2200665.
[41] J. S. Jang, S. H. Han, H. W. Choi, K. S. Yook, J. Y. Lee, *Org. Electron.* **2018**, *59*, 236.
[42] H. Mubarok, A. Amin, T. Lee, J. Jung, J.-H. Lee, M. H. Lee, *Angew. Chem., Int. Ed.* **2023**, *62*, 202306879.
[43] K. H. Lee, J. Y. Lee, *J. Mater. Chem. C* **2019**, *7*, 8562.
[44] B. W. D'Andrade, M. A. Baldo, C. Adachi, J. Brooks, M. E. Thompson, S. R. Forrest, *Appl. Phys. Lett.* **2001**, *79*, 1045.
[45] K. Klimes, Z. Q. Zhu, J. Li, *Adv. Funct. Mater.* **2019**, *29*, 1903068.
[46] J. Yan, Y. Xin, Y. Pan, G. Ni, S.-M. Yiu, Y. Chi, L. Duan, K. C. Lau, *Synth. Met.* **2024**, *308*, 117734.
[47] C.-Y. Chan, M. Tanaka, Y.-T. Lee, Y.-W. Wong, H. Nakanotani, T. Hatakeyama, C. Adachi, *Nat. Photonics* **2021**, *15*, 203.
[48] H.-H. Cho, D. G. Congrave, A. J. Gillett, S. Montanaro, H. E. Francis, V. Riesgo-Gonzalez, J. Ye, R. Chowdury, W. Zeng, M. K. Etherington,

J. Royakkers, O. Millington, A. D. Bond, F. Plasser, J. M. Frost, C. P. Grey, A. Rao, R. H. Friend, N. C. Greenham, H. Bronstein, *Nat. Mater.* **2024**, *23*, 519.
[49] Z.-L. Zhu, J. Yan, L.-W. Fu, C. Cao, J.-H. Tan, S.-F. Wang, Y. Chi, C.-S. Lee, *Mater. Chem. Front.* **2023**, *7*, 3398.
[50] A. Cravcenco, M. Hertzog, C. Ye, M. N. Iqbal, U. Mueller, L. Eriksson, K. Börjesson, *Sci. Adv.* **2019**, *5*, 5978.
[51] H. W. Son, D. I. Kim, J. H. Kim, T. N. Le, Y.-H. Kim, M. C. Suh, *J. Ind. Eng. Chem.* **2025**, *141*, 512.
[52] T. Hatakeyama, K. Shiren, K. Nakajima, S. Nomura, S. Nakatsuka, K. Kinoshita, J. Ni, Y. Ono, T. Ikuta, *Adv. Mater.* **2016**, *28*, 2777.
[53] S. S. Madayanad, D. Hall, D. Beljonne, Y. Olivier, E. Zysman-Colman, *Adv. Funct. Mater.* **2020**, *30*, 1908677.
[54] K. R. Naveen, P. Palanisamy, M. Y. Chae, J. H. Kwon, *Chem. Commun.* **2023**, *59*, 3685.
[55] X.-F. Luo, X. Xiao, Y.-X. Zheng, *Chem. Commun.* **2024**, *60*, 1089.
[56] Y. Zhang, D. Zhang, J. Wei, X. Hong, Y. Lu, D. Hu, G. Li, Z. Liu, Y. Chen, L. Duan, *Angew. Chem., Int. Ed.* **2020**, *59*, 17499.
[57] X.-C. Fan, F. Huang, H. Wu, H. Wang, Y.-C. Cheng, J. Yu, K. Wang, X.-H. Zhang, *Angew. Chem., Int. Ed.* **2023**, *62*, 202305580.
[58] X. Cai, Y. Xu, Y. Pan, L. Li, Y. Pu, X. Zhuang, C. Li, Y. Wang, *Angew. Chem., Int. Ed.* **2023**, *62*, 202216473.
[59] T. Hua, N. Li, Z. Huang, Y. Zhang, L. Wang, Z. Chen, J. Miao, X. Cao, X. Wang, C. Yang, *Angew. Chem., Int. Ed.* **2024**, *63*, 202318433.
[60] X. Cai, Y. Pu, C. Li, Z. Wang, Y. Wang, *Angew. Chem., Int. Ed.* **2023**, *62*, 202304104.
[61] G. Li, J. Ecton, B. O'Brien, J. Li, *Org. Electron.* **2014**, *15*, 1862.
[62] E. Kim, J. Park, M. Jun, H. Shin, J. Baek, T. Kim, S. Kim, K. Lee, H. Ahn, J. Sun, S.-B. Ko, S.-H. Hwang, J. Y. Lee, C. Chu, S. Kim, *Sci. Adv.* **2022**, *8*, 1641.
[63] J. Choi, K. Cheong, S. Han, J. Y. Lee, *Adv. Opt. Mater.* **2024**, *12*, 2401451.
[64] J. Sun, H. Ahn, S. Kang, S.-B. Ko, D. Song, H. A. Um, S. Kim, Y. Lee, P. Jeon, S.-H. Hwang, Y. You, C. Chu, S. Kim, *Nat. Photonics* **2022**, *16*, 212.
[65] K. Cheong, U. Jo, W. P. Hong, J. Y. Lee, *Small Methods* **2024**, *8*, 2300862.
[66] L. Graf von Reventlow, M. Koodalingam, C. Siebert, P. Marlow, E. V. Puttock, P. L. Burn, A. Colsmann, *J. Mater. Chem. C* **2022**, *10*, 8278.
[67] D. Wang, C. Cheng, T. Tsuboi, Q. Zhang, *CCS Chem.* **2020**, *2*, 1278.
[68] J. Jiang, J. Y. Lee, *Mater. Today* **2023**, *68*, 204.
[69] E. V. Puttock, M. T. Walden, J. A. G. Williams, *Coord. Chem. Rev.* **2018**, *367*, 127.
[70] K.-W. Lo, G. S. M. Tong, G. Cheng, K.-H. Low, C.-M. Che, *Angew. Chem., Int. Ed.* **2022**, *61*, 202115515.
[71] Z.-L. Zhu, P. Gnanasekaran, J. Yan, Z. Zheng, C.-S. Lee, Y. Chi, X. Zhou, *Inorg. Chem.* **2022**, *61*, 8898.
[72] J. Yan, Z.-H. Qu, D.-Y. Zhou, S.-M. Yiu, Y. Qin, X. Zhou, L.-S. Liao, Y. Chi, *ACS Appl. Mater. Interfaces* **2024**, *16*, 3809.
[73] Y. Wu, K.-N. Tong, M. Kuhn, C. Wu, W.-Y. Hung, G. Wei, J. Yan, Y. Chi, X. Zhou, *J. Mater. Chem. C* **2025**, *13*, 3501.
[74] J. Yan, T. Nakamura, X. Tan, S.-M. Yiu, R. Mimura, K. Hoshi, X. Zhou, Y. Chi, H. Sasabe, J. Kido, *J. Chem. Eng.* **2024**, *488*, 150791.
[75] J. Yan, Z.-Q. Feng, Y. Wu, D.-Y. Zhou, S.-M. Yiu, C.-Y. Chan, Y. Pan, K. C. Lau, L.-S. Liao, Y. Chi, *Adv. Mater.* **2024**, *36*, 2305273.
[76] X. Yang, X. Zhou, Y.-X. Zhang, D. Li, C. Li, C. You, T.-C. Chou, S.-J. Su, P.-T. Chou, Y. Chi, *Adv. Sci.* **2022**, *9*, 2201150.
[77] J. Yan, C. Wu, S. M. Yiu, M. Kuhn, M. Huang, Y. Zhang, X. Zhou, C. Yang, G. Wei, Y. Chi, *Adv. Opt. Mater.* **2025**, *13*, 2402332.
[78] J. Yan, S. F. Wang, C.-H. Hsu, E. H.-C. Shi, C.-C. Wu, P.-T. Chou, S.-M. Yiu, Y. Chi, C. You, I.-C. Peng, W.-Y. Hung, *ACS Appl. Mater. Interfaces* **2023**, *15*, 21333.
[79] Y. Qin, X. Yang, J. Jin, D. Li, X. Zhou, Z. Zheng, Y. Sun, W. Y. Wong, Y. Chi, S. J. Su, *Adv. Opt. Mater.* **2022**, *10*, 201633.
[80] Y. Wu, Y. Xin, Y. Pan, S. M. Yiu, J. Yan, K. C. Lau, L. Duan, Y. Chi, *Adv. Sci.* **2024**, *11*, 2309389.
[81] Z. Zheng, L. Wang, Y. Xin, Q. Wang, X. Hong, Y. Zhang, S. M. Yiu, F. Zhou, J. Yan, D. Zhang, L. Duan, Y. Chi, *Adv. Funct. Mater.* **2024**, 2311692.
[82] J. Jin, Z. Zhu, J. Yan, X. Zhou, C. Cao, P.-T. Chou, Y.-X. Zhang, Z. Zheng, C.-S. Lee, Y. Chi, *Adv. Photonics Res.* **2022**, *3*, 2100381.
[83] J. Yan, Y. Wu, I. C. Peng, Y. Pan, S.-M. Yiu, K.-T. Wong, W.-Y. Hung, Y. Chi, K.-C. Lau, *J. Mater. Chem. C* **2023**, *11*, 12270.
[84] J. Yan, Y. Pan, Z. H. Qu, Z. Xu, K. C. Law, D. Y. Zhou, L. S. Liao, Y. Chi, K. C. Lau, *Adv. Photonics Res.* **2024**, 2400151.
[85] J. Yan, Q. Xue, H. Yang, S.-M. Yiu, Y.-X. Zhang, G. Xie, Y. Chi, *Inorg. Chem.* **2022**, *61*, 8797.
[86] J. Yan, Y. Pan, I. C. Peng, W.-Y. Hung, B. Hu, G. Ni, S.-M. Yiu, Y. Chi, K. C. Lau, *Inorg. Chem. Front.* **2024**, *11*, 2413.
[87] J. Yan, C. Wu, K.-N. Tong, F. Zhou, Y. Chen, Y. Pan, G. Xie, Y. Chi, K.-C. Lau, G. Wei, *Small Methods* **2024**, *8*, 2301555.
[88] W. J. Chung, K. H. Lee, M. Jung, K. M. Lee, H. C. Park, M. S. Eum, J. Y. Lee, *Adv. Opt. Mater.* **2021**, *9*, 2100203.
[89] P. Palanisamy, O. P. Kumar, H. U. Kim, K. R. Naveen, J.-Y. Kim, J.-H. Baek, M. Y. Chae, J. H. Kwon, *J. Chem. Eng.* **2024**, *481*, 148781.
[90] X. Song, Y. Nie, C. Jiang, B. Liang, J. Liang, X. Zhuang, H. Bi, Y. Wang, *Org. Electron.* **2024**, *125*, 106973.
[91] T. Sajoto, P. I. Djurovich, A. B. Tamayo, J. Oxgaard, W. A. Goddard, M. E. Thompson, *J. Am. Chem. Soc.* **2009**, *131*, 9813.
[92] D. Zhang, M. Cai, Y. Zhang, D. Zhang, L. Duan, *Mater. Horiz.* **2016**, *3*, 145.
[93] J. Dong, Y. Xu, S. Wang, J. Miao, N. Li, Z. Huang, C. Yang, *Chem. Commun.* **2024**, *60*, 6789.
[94] T. Fan, M. Du, X. Jia, L. Wang, Z. Yin, Y. Shu, Y. Zhang, J. Wei, D. Zhang, L. Duan, *Adv. Mater.* **2023**, *35*, 2301018.
[95] H. Li, C. Chen, Z. Ye, K. Feng, J. Huang, G. Xie, Y. Tao, *FlexMat* **2024**, *1*, 173.
[96] X. Peng, P. Zou, J. Zeng, X. Wu, D. Xie, Y. Fu, D. Yang, D. Ma, B. Z. Tang, Z. Zhao, *Angew. Chem., Int. Ed.* **2024**, *63*, 202405418.
[97] J. Zeng, S. Song, Y. Gu, X. Peng, B. Z. Tang, Z. Zhao, *Sci. Adv.* **2025**, *11*, 7899.
[98] L. Xu, Y. Mo, N. Su, C. Shi, N. Sun, Y. Zhang, L. Duan, Z.-H. Lu, J. Ding, *Nat. Commun.* **2023**, *14*, 1678.
[99] J. Ding, L. Xu, S. Xiao, Y. Yang, N. Su, C. Shi, H. Ding, N. Sun, L. Ding, *Res. Square* **2025**, https://doi.org/10.21203/rs.3.rs-5497779/v1.

Emma V. Puttock obtained her Ph.D. from Durham University in 2017. She subsequently held postdoctoral positions at The University of Queensland (2017–2021) and Durham University (2021–2023) before joining KIT in 2023 as a Marie Skłodowska-Curie fellow. Her research focuses on the design of advanced emitters for solution-processed OLEDs, including (MR-)TADF and phosphorescent materials, with a particular interest in HyperOLED systems to enhance efficiency, achieve narrowband emission, and improve the sustainability of next-generation optoelectronic devices.

Janine Haug obtained her B.Sc. degree in chemical biology from the KIT in 2021. After a research stay in the group of Prof. E. Zysman-Colman (University of St Andrews, Scotland) working on MR-TADF materials for OLEDs, she received her M.Sc. degree in 2023. Subsequently, she started her Ph.D. studies cosupervised by Prof. S. Bräse (KIT) and Prof. E. Zysman-Colman, focusing on the development of TADF materials for OLEDs and biomedical applications.

Eli Zysman-Colman obtained his Ph.D. from McGill University in 2003. He then completed two postdoctoral fellowships, one at the University of Zurich and the other at Princeton. He joined the Université de Sherbrooke in Quebec, Canada as an assistant professor in 2007. In 2013, he moved to the University of St Andrews, UK, where he is presently Professor of Optoelectronic Materials, and an EPSRC open fellow. His research program focuses on the rational design of I) materials for electroluminescent devices, II) sensing materials, III) optical imaging agents, and IV) photocatalyst development for use in organic synthetic reactions.

Stefan Bräse studied chemistry in Göttingen, Bangor, and Marseille, earning his Ph.D. in 1995 in Göttingen. After postdoctoral research at Uppsala and the Scripps Research (with K.C. Nicolaou), he began independent research at the RWTH Aachen in 1997 and was promoted to professor in Bonn in 2001. Since 2003, he has been a professor at the Institute of Organic Chemistry, Karlsruhe Institute of Technology (KIT), and since 2012, also the Director of the Institute of Biological and Chemical Systems (IBCS-FMS) at the KIT. His research interests include synthetic chemistry, molecular engineering of functional synthetic materials, and digitization in chemistry.